(21)

A TRIDENT SCHOLAR PROJECT REPORT

NO. 209

DELAMINATION IN COMPOSITE MATERIALS AS OBSERVED USING AN OPTICAL FIBER STRAIN GAGE

UNITED STATES NAVAL ACADEMY
ANNAPOLIS, MARYLAND

DELAMINATION IN COMPOSITE MATERIALS AS OBSERVED USING AN OPTICAL FIBER STRAIN GAGE

by
Midshipman Glen E. Sabin, Class of 1993
U.S. Naval Academy
Annapolis, Maryland

Olaf N. Rask

Advisor: Associate Prof. Olaf N. Rask
Weapons and Systems Engineering Department

Accepted for Trident Scholar Committee

Francis DeCorrell
Chair

May 17, 1993
Date

REPORT DOCUMENTATION PAGE

Form Approved
OMB no. 0704-0188

1. AGENCY USE ONLY (Leave blank)	2. REPORT DATE	3. REPORT TYPE AND DATES COVERED
	May 17, 1993	

4. TITLE AND SUBTITLE

Delamination in composite materials as observed using an optical fiber strain gage

5. FUNDING NUMBERS

6. AUTHOR(S)

Glen Edward Sabin

7. PERFORMING ORGANIZATIONS NAME(S) AND ADDRESS(ES)

U.S. Naval Academy, Annapolis, MD

8. PERFORMING ORGANIZATION REPORT NUMBER

U.S.N.A. - Trident scholar project report ; no. 209

9. SPONSORING/MONITORING AGENCY NAME(S) AND ADDRESS(ES)

10. SPONSORING/MONITORING AGENCY REPORT NUMBER

11. SUPPLEMENTARY NOTES

Accepted by the U.S. Trident Scholar Committee

12a. DISTRIBUTION/AVAILABILITY STATEMENT

This document has been approved for public release; its distribution is UNLIMITED.

12b. DISTRIBUTION CODE

13. ABSTRACT (Maximum 200 words)

Composite materials are used extensively in the air and space industries, where materials of high strength and light weight are required. Unlike metals, these materials often give little or no warning before failing–a potentially fatal characteristic for structural members in aircraft. A common mode of failure in composites is delamination, in which the layers of the material separate from each other. Delamination can be caused by impact, longitudinal shear stress between the layers, or transverse tensile stress across the layers. Optical fibers embedded in the composite material provide a means of monitoring the strains which lead to such failures.

This project involves the use of an optical fiber strain gage in the configuration of a Michelson interferometer to study a composite sample that experiences transverse tensile stress resulting in delamination. The transverse tensile stress is produced by straightening out an already curved specimen of composite material. The output signal of the interferometer represents the integrated strain over the length of the optical fibers. By embedding the fibers in a composite specimen, the strain experienced in the material can be measured. This signal is recorded on an common audio tape, transferred to a computer, and analyzed quantitatively.

14. SUBJECT TERMS	15. NUMBER OF PAGES
composite materials, delamination, optical fiber strain gage	64
	16. PRICE CODE

17. SECURITY CLASSIFICATION OF REPORT	18. SECURITY CLASSIFICATION OF THIS PAGE	19. SECURITY CLASSIFICATION OF ABSTRACT	20. LIMITATION OF ABSTRACT
UNCLASSIFIED	UNCLASSIFIED	UNCLASSIFIED	UNCLASSIFIED

Abstract

Composite materials are used extensively in the air and space industries, where materials of high strength and light weight are required. Unlike metals, these materials often give little or no warning before failing--a potentially fatal characteristic for structural members in aircraft. A common mode of failure in composites is delamination, in which the layers of the material separate from each other. Delamination can be caused by impact, longitudinal shear stress between the layers, or transverse tensile stress across the layers. Optical fibers embedded in the composite material provide a means of monitoring the strains which lead to such failures.

This project involves the use of an optical fiber strain gage in the configuration of a Michelson interferometer to study a composite sample that experiences transverse tensile stress resulting in delamination. The transverse tensile stress is produced by straightening out an already curved specimen of composite material. The output signal of the interferometer represents the integrated strain over the length of the optical fibers. By embedding the fibers in a composite specimen, the strain experienced in the material can be measured. This signal is recorded on a common audio tape, transferred to a computer, and analyzed quantitatively.

Keywords: Composite materials, Delamination, Optical Fiber Strain Gage

Table of Contents

Introduction.....3

Specimen Configuration.....5

Specimen Preparation.....7

Test Apparatus.....10

Optical Strain Gage Configuration.....12

Construction of Michelson Interferometer.....22

Optical Fringe Generation.....27

Electronic Signal Processing.....28

Results.....30

Applications.....35

Future Work.....35

Bibliography.....38

Appendices.....40

Introduction

Composite materials are defined to be those materials which are made up of at least two distinct phases and which have useful properties superior to those of either phase. There are natural composites such as wood and bone, and artificial composites like concrete and fiber/resin systems. Fiber/resin composite materials offer several advantages over traditional structural materials such as wood and metal. Specifically, composites are very stiff and strong for their weight, and they are easily molded into different shapes. These characteristics make fiber/resin composites especially useful in aircraft, boats, and other applications where weight is a consideration. The strength of a fiber/resin composite comes mainly from the fibers. Fibers typically used in composite materials include glass, kevlar, and carbon.[1] It has been shown that fibers can withstand more force per unit area than larger bulks of the same material. This is because the small cross-sectional area of the fibers does not allow the formation of the small cracks and flaws that often lead to failures in larger specimens.[2] However, fibers alone are not useful for building structures because they easily bend and

---

[1] Marine Composites, Eric Greene Associates, (1990), p. 43.

[2] A.A. Griffith, "The Phenomena of Rupture and Flow in Solids," Philosophical Transactions Royal Society (London), Vol. 221 (Oct., 1920).

buckle when compressed. To form a useful material, the fibers are placed in a mold and impregnated with liquid resin, and the resin is allowed to harden. Common resins used in composites include epoxy, vinyl ester, and polyester.[3]

Fiber/resin composites do have important disadvantages. These materials tend to be brittle and to give little or no warning before failing. Because fiber/resin composites are relatively new, their failure modes and their deterioration with time and fatigue are not completely understood and are presently under active study. One important failure mode is that of delamination. Fiber/resin systems are usually, but not always, made up of distinct layers of fibers impregnated with resin.[4] These layers range in configuration from weaves and knits to unidirectional tapes. Delamination occurs when the resin holding these layers together fails, and the layers come apart. When this happens, the support of the fibers in compression is markedly reduced, which in turn reduces the strength and stiffness of the structure. Aeroelastic instabilities are promoted by a reduction in stiffness. Such damage in the wing of the AV-8B Harrier is so serious that if a tool is accidentally dropped onto its composite wing, the aircraft is grounded until it can be checked for delamination.

---

[3]Marine Composites, pp. 47-48.

[4]Bhagwan D. Agarwal and Lawrence J. Broutman, Analysis and Performance of Fiber Composites, (New York: John Wiley & Sons, Inc., 1990), pp. 8-9.

Specimen Configuration

In order to delaminate a composite specimen, stress must be applied to the interlaminar resin. When a beam is bent as shown in Figure 1, the longitudinal interlaminar shear stress is a maximum in the center of the beam. This stress is shown in Appendix A to be that given in Equation 1.

$$\tau = (\frac{3}{2}) * (\frac{V}{A}) \qquad (1)$$

Here, V is the transverse shear force across the beam and A is the cross sectional area of the beam. That is, the longitudinal interlaminar shear stress is 3/2 of the transverse shear stress. In the early stages of this project, many straight beam specimens were produced and tested. However, the failure mode for these specimens was quite complex and did not consist of pure delamination. Several attempts were made to promote pure delamination. Pieces of wax paper were added between the layers in one case, and some fibers were coated with a liquid mold release agent in another. However, the flat beam specimens were never observed to fail in pure delamination.

A study of the literature revealed that other investigators had solved this problem with the use of curved

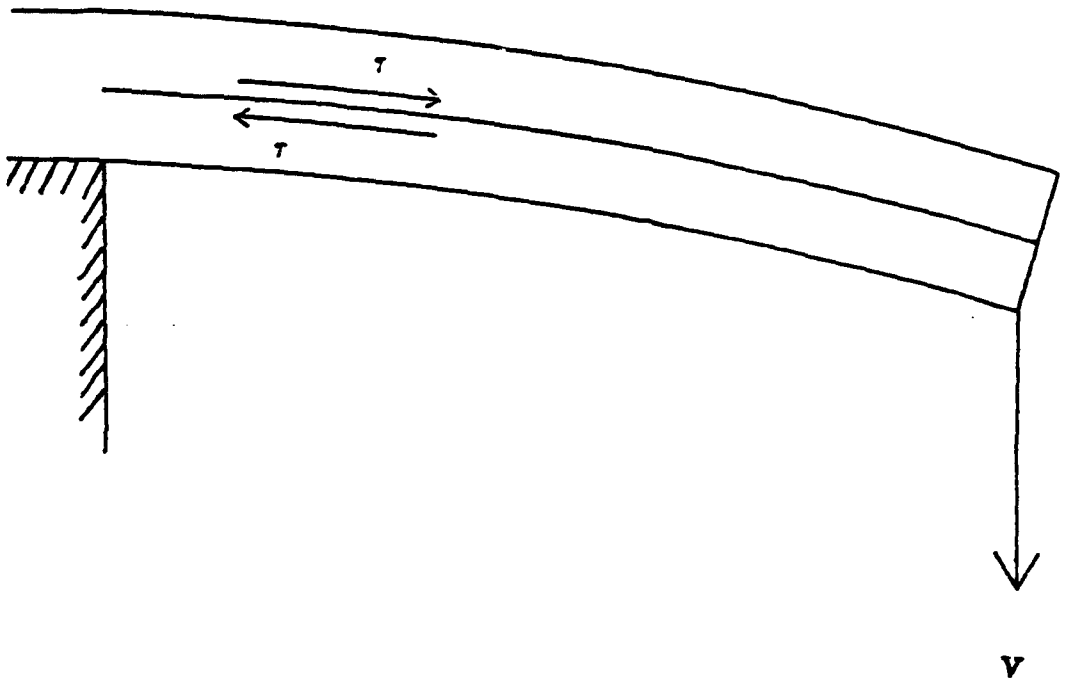

Figure 1. Longitudinal shear stress of normally straight beam caused by a force V

specimens.[5] Such a specimen is illustrated in Figure 2. The specimens used in this project are elliptical with major and minor axes as shown. In Appendices B, C, and D, the transverse interlaminar stress is shown to be a maximum in the center, and given by the expression in Equation 2.

$$\sigma_T = \left(\frac{3}{2}\right) * \left(\frac{V}{A}\right) * \left(\frac{b^2}{a^2}\right) \qquad (2)$$

Therefore, the use of an elliptical specimen with b > a results in increased stress over a straight beam specimen for the same applied force. The observed failure mode for these specimens was always pure delamination.

Specimen Preparation

The construction of the specimens involves the lay-up of fourteen layers of unidirectional fiberglass tape on an elliptical form as shown in Figure 3. The elliptical form was cut from a block of high density foam and covered with vinyl tape treated with a liquid mold release agent so that the finished specimens would not stick to it. To build the structure, fourteen layers of fiberglass tape are draped over the form and saturated with epoxy resin, one layer at a time. Finally, a piece of peel ply is placed on top of the fibers to soak up any excess resin and to give the specimens a smooth

---

[5]M. Sumich, "Manufacture of Composite Test Specimens for Delamination Studies," Experimental Techniques, Vol. 13 (Oct. 1989), pp. 20-22.

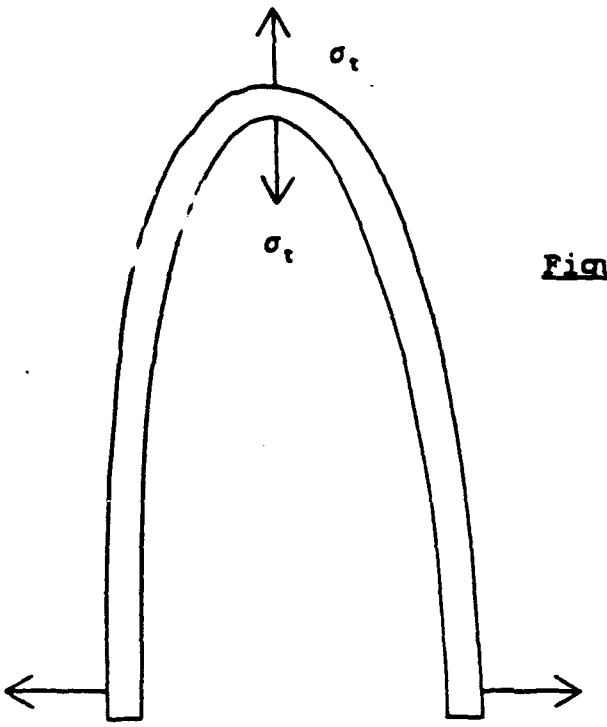

Figure 2a. Transverse tensile stess in a normally curved beam caused by a force V

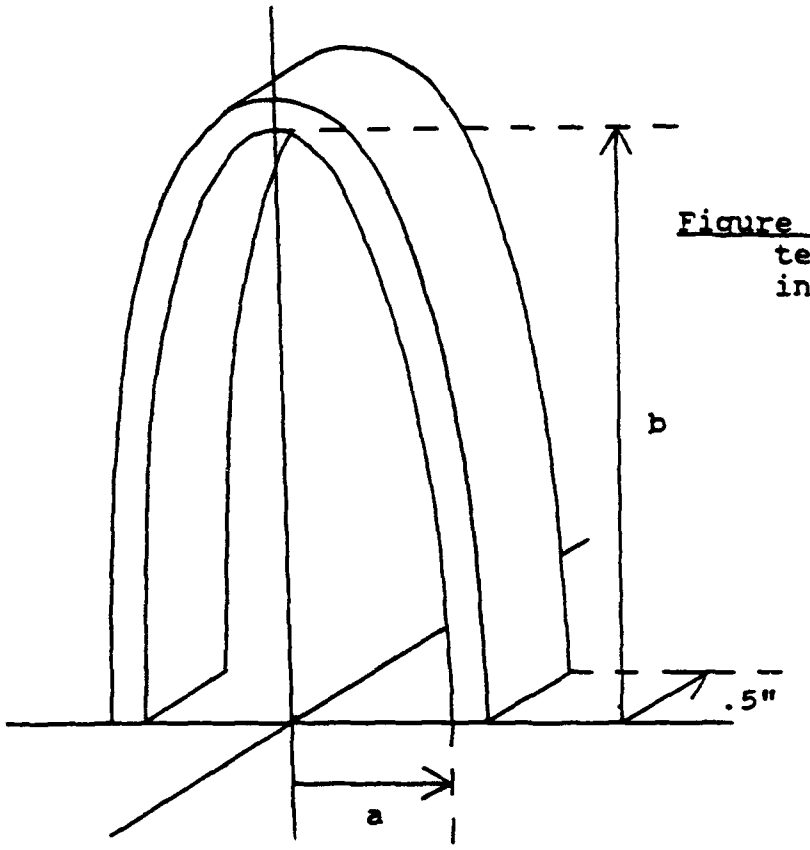

Figure 2b. Elliptical test specimen used in this project

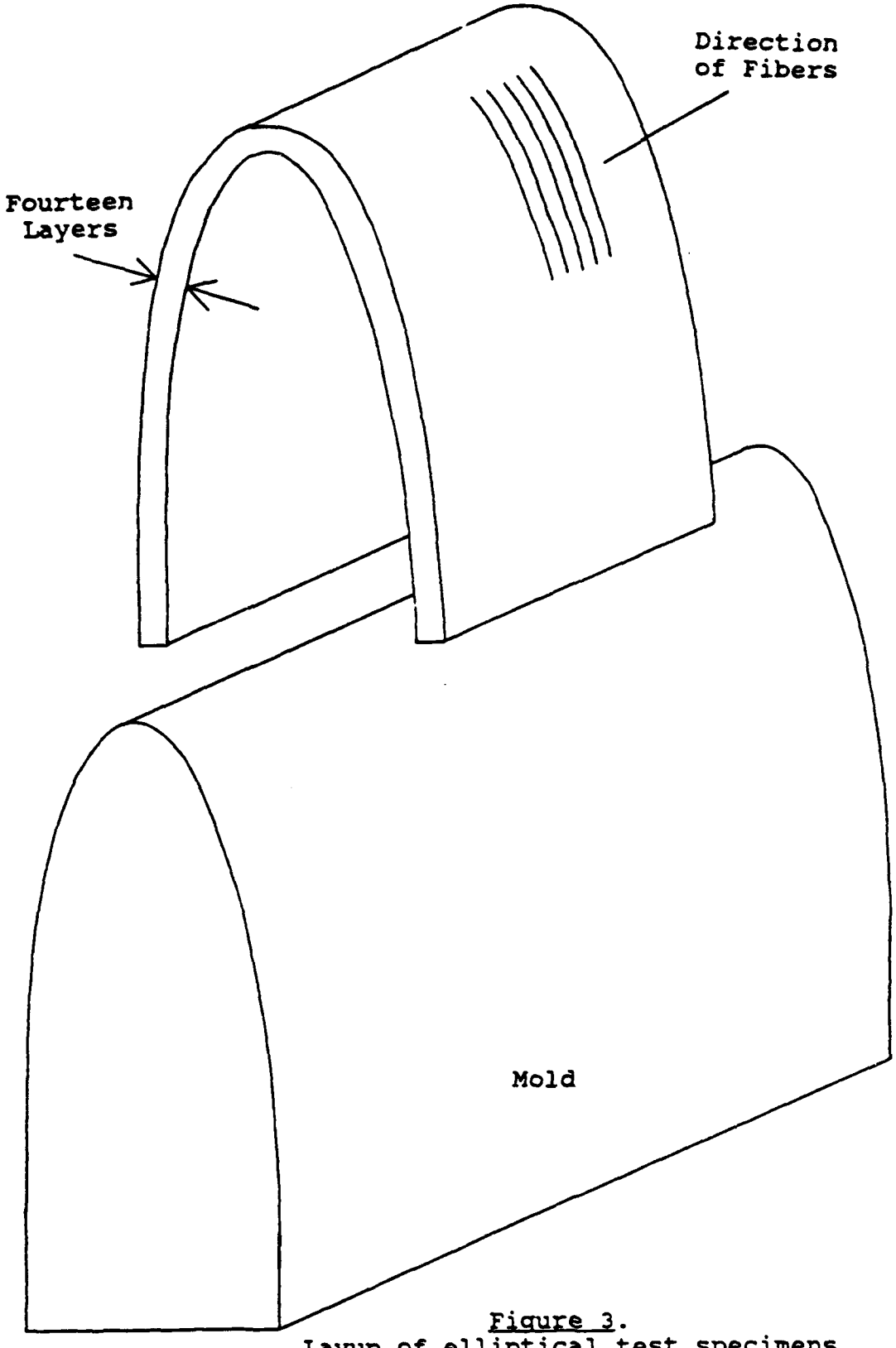

Figure 3.
Layup of elliptical test specimens

outer surface. After the resin had hardened, the individual specimens, one half inch wide, were cut from the structure. One-inch-long steel rods were epoxied to the ends of the specimens to accommodate the test apparatus used to cause delamination.

Test Apparatus

In order to study delamination in the elliptically shaped specimens, it is necessary to have a device that can cause the failure to occur in a controlled and measurable way. The apparatus used in this project is shown in Figure 4. Here, the steel rods on the ends of the specimens are used to clamp the samples to two blocks. One of these blocks is fixed in a track on the base of the device, while the other is threaded onto a screw as shown. The pitch of the screw is sixteen turns per inch. By turning the handle on the end of the screw, the two legs of the specimen can be pulled a known distance apart.

This apparatus can be easily altered to apply a known force to the specimen rather than a known displacement. This is done by adding a spring between the threaded block and the leg of the specimen. The force can be determined by measuring how far the spring is stretched. No experiments with this configuration were carried out for this project.

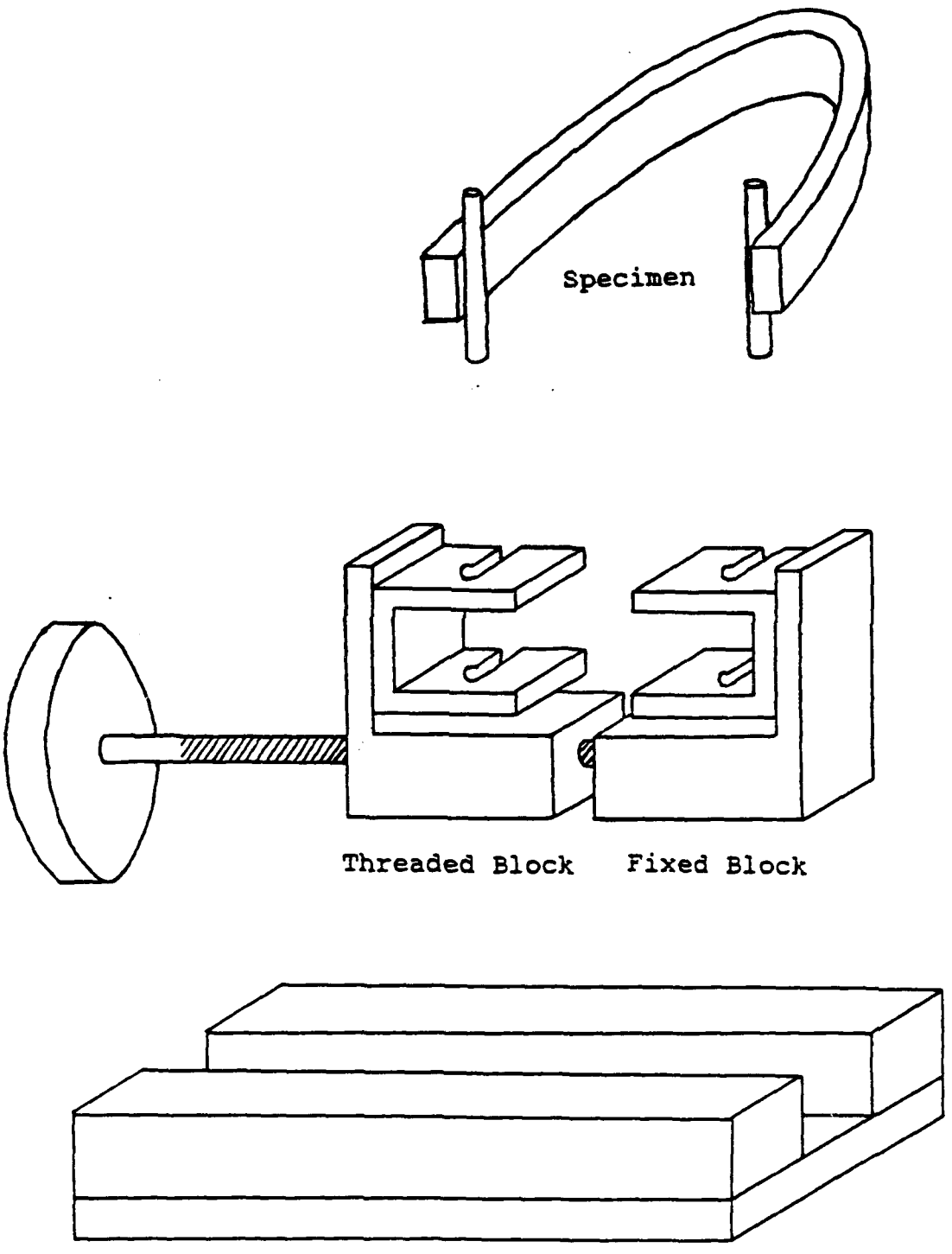

Figure 4. Test Apparatus

Optical Strain Gage Configuration

A 1991 Trident Scholar Project by Midshipman Daniel Robinson proved that optical fibers could be used effectively to monitor the strain and structural integrity of composite specimens.[6] Optical fibers are small in diameter, and are similar to the glass fibers used to build the composite material used in this project. Therefore, unlike conventional foil strain gages, they can be embedded into a composite specimen without significantly affecting the properties of the material.

The composition of an optical fiber is shown in Figure 5. Optical fibers work by a process called total internal reflection.[7] There is a difference in the index of refraction between the cladding of the fiber and the core. When the light in the core reaches the boundary between the two, it is reflected back towards the core, so that none of the light escapes. The jacket provides protection for the fiber.

An additional component used with optical fibers is a bidirectional coupler. This device consists of two fibers

---

[6]Daniel B. Robinson, "Optical Strain Monitoring in Composite Materials," Trident Scholar Project Report No. 186, U.S. Naval Academy (1991).

[7]Projects in Fiber Optics: Applications Handbook, Newport Corporation, (1986), pp. 6-7.

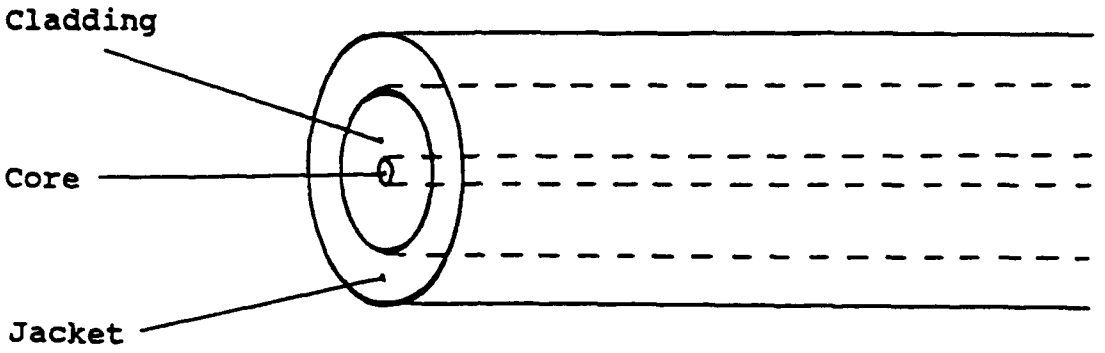

Figure 5. Composition of an optical fiber

placed very close together as shown in Figure 6.[8] By a process called frustrated total internal reflection, the light that enters the coupler at one end on a single fiber exits at the other end on both fibers. If light comes in at one end on two fibers, then the light in both of these fibers is summed and exits at the other end on both fibers.

Optical fibers are used as sensors because they offer a means of forcing light to follow a certain path within a specimen. They can be arranged into a device called an interferometer. An interferometer simply separates light from a single source into two different paths using the bidirectional coupler. These paths are termed the arms of the interferometer. When the light from the two arms is later recombined in another bidirectional coupler, the resulting sum will demonstrate interference effects which depend on the relative lengths of the two arms. Optical sensors use mainly three different interferometer configurations. Figure 7 shows them in their original configuration, consisting of light beams travelling in the open air. Figure 8 shows the optical fiber equivalents of these same three interferometer forms. If the fibers in the arms of an interferometer are attached to different portions of a composite specimen, the results of the work by Robinson show that optical fibers experience the same strain as the portion of the specimen through which the fibers

---

[8]Projects in Fiber Optics: Applications Handbook, p. 72.

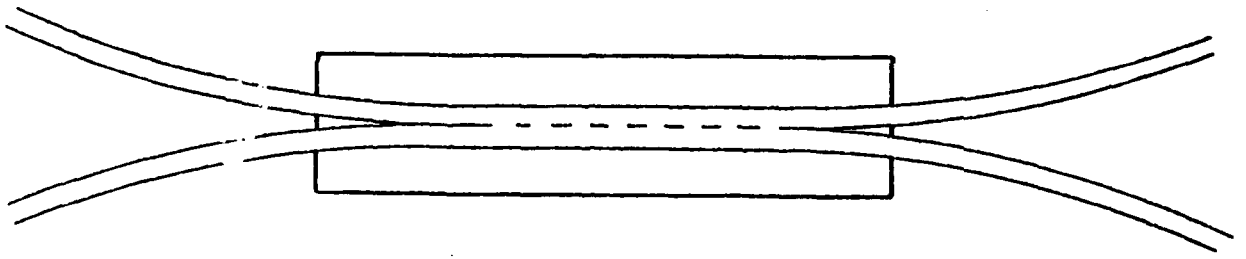

Figure 6. Bidirectional coupler used in optical fiber interferometers

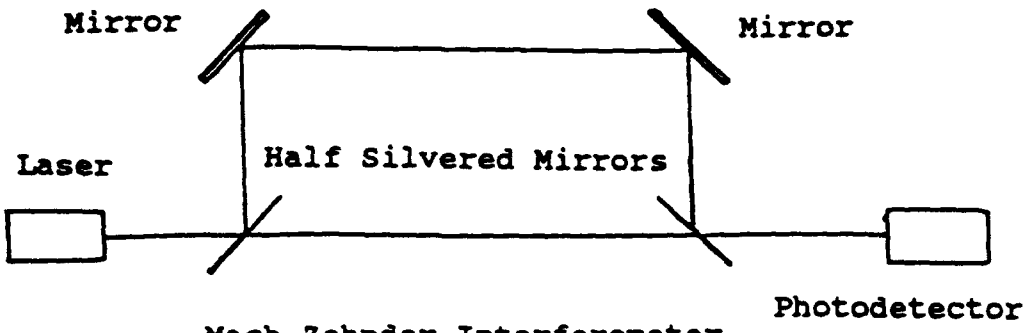

Mach-Zehnder Interferometer

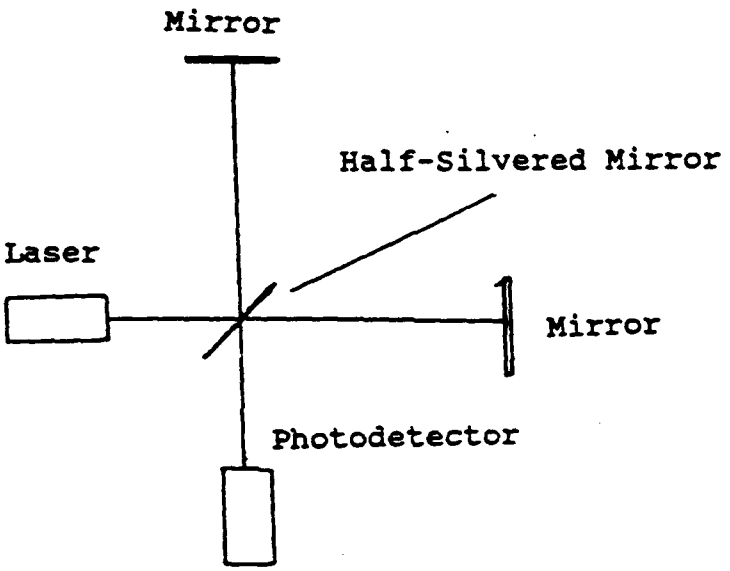

Michelson Interferometer

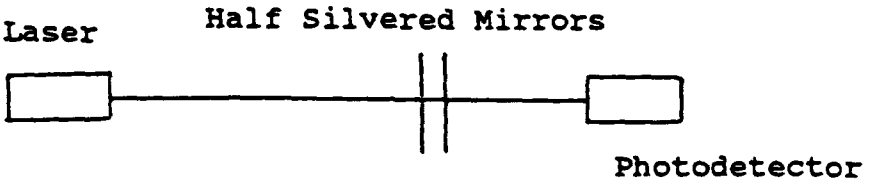

Fabry-Perot Interferometer

Figure 7. Traditional interferometeter configurations

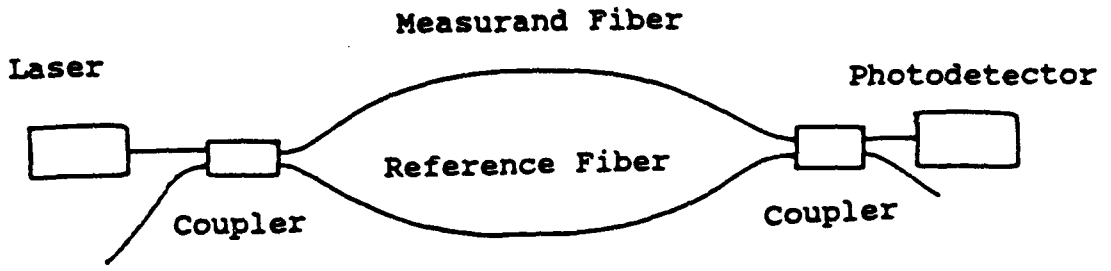

Mach-Zehnder Interferometer

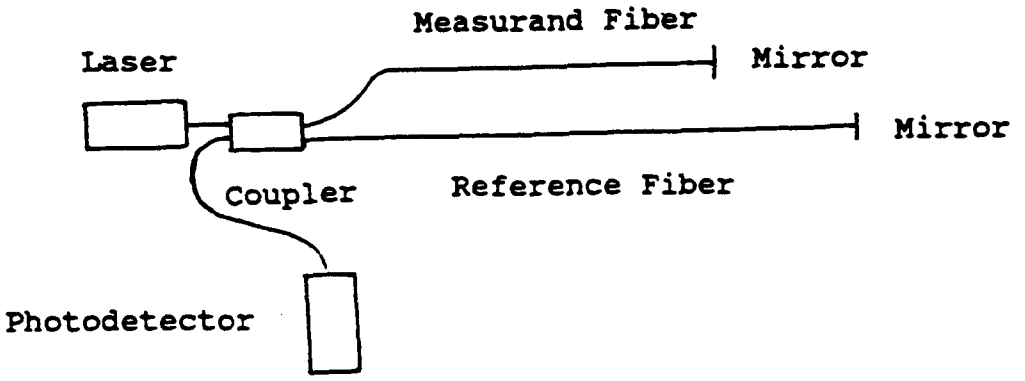

Michelson Interferometer

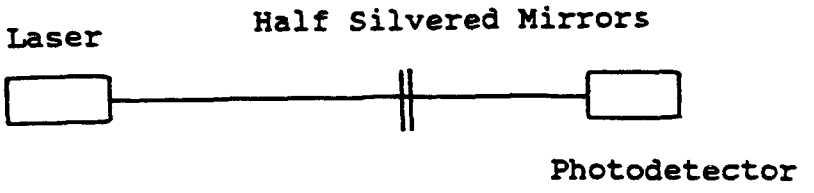

Fabry-Perot Interferometer

Figure 8. Optical fiber interferometer configurations

pass. In this way the fibers can be used to monitor the relative strains.

Midshipman Robinson's Trident Scholar Project involved the use of the fiber optic equivalent of a Mach-Zehnder interferometer, as shown in Figure 9.[9] His work with a straight specimen in simple three point bending proved that an optical fiber strain gage could provide data similar in accuracy to a traditional foil type strain gage. Although his setup worked well for the repeated study of a single specimen, it proved to be not the best configuration for the present work. This is because it is very difficult to maintain linearly polarized light in the output fiber and to change the specimen being studied.

The state of polarization of the light at the output of the interferometer affects the clarity of the interference fringes caused by the strain in the specimen. Even though the light from the input source, a helium-neon laser, is linearly polarized, the output may be elliptically polarized, or even circularly polarized. This is because the polarization of the light in the two optical paths of the interferometer changes with the twists and turns of the fibers that carry it. The polarization of the light in each path is rotated by an unknown and different angle. When the light from the two paths is recombined in the second bidirectional coupler, there is an excellent chance that the two signals are not polarized

---

[9]Robinson, pp. 6-7.

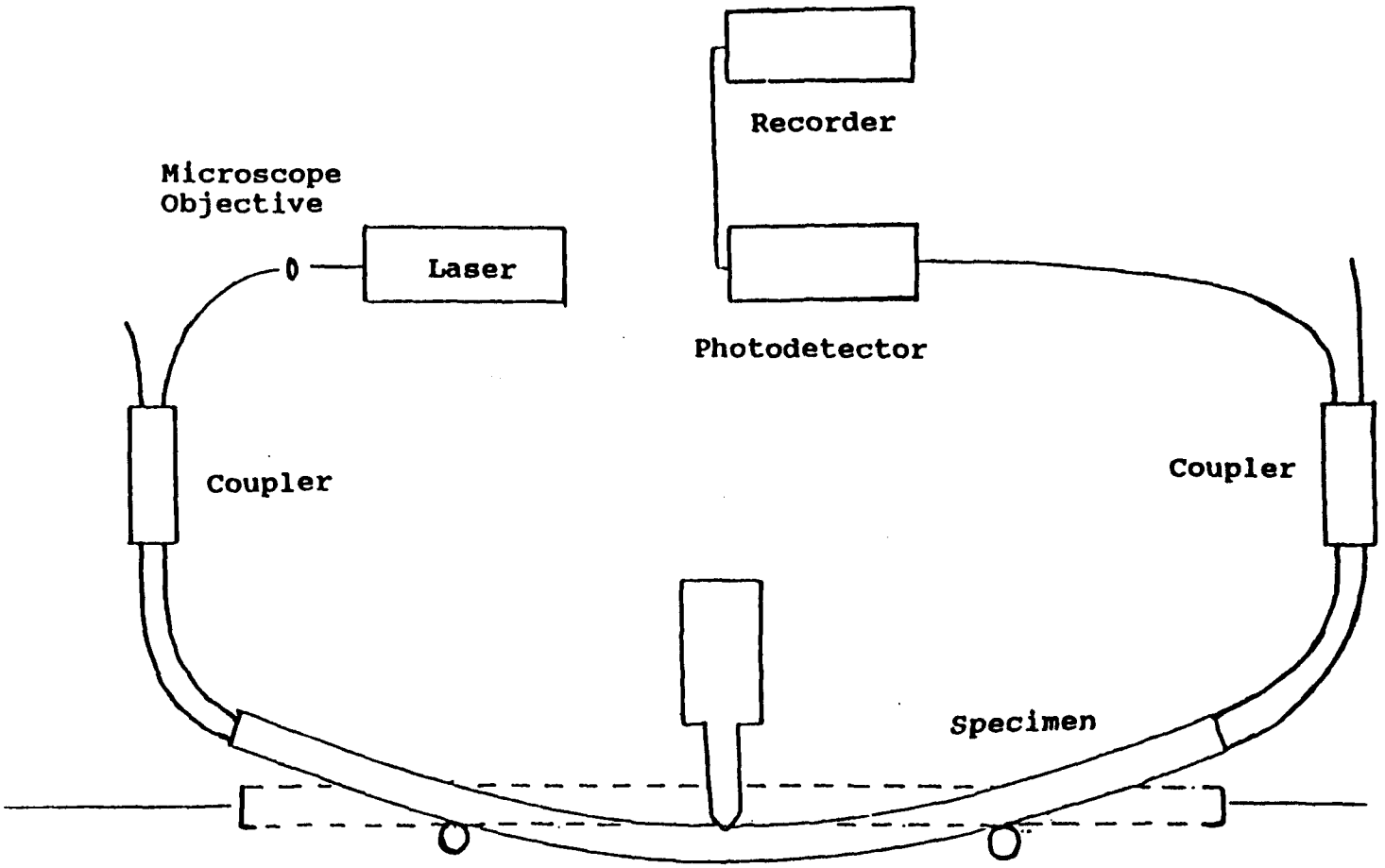

Figure 9. Optical fiber strain gage in configuration of Mach-Zehnder interferometer as used in Midshipman Robinson's Trident Scholar project

in the same plane, resulting in an output signal that is not linearly polarized. If the output fiber carries circularly polarized light, then no interference fringes will be seen. The output from the photodetector will be constant. The closer the output light is to being linearly polarized, the more visible the interference fringes are. To solve this problem using the Mach-Zehnder setup, it is necessary to bend one of the fibers using a polarization adjusting device until the interference fringes are easily detectable.

The second problem is the difficulty in changing the test specimen. When the failure of composite materials is studied, as in this project, the test specimens cannot be reused. Once the specimen is broken, it must be replaced. Because the fibers cannot be removed from a specimen without damaging them, it would have been necessary to break fibers in four places to remove a specimen from the Mach-Zehnder interferometer. This means that it would be necessary to make four fusions of fibers to put in another specimen to be tested. With the facilities available for use with this project, it was very difficult to connect optical fibers. It is also not feasible to build an entirely new interferometer for each specimen, as two expensive bidirectional couplers are then needed for each test.

These two problems were overcome by using the fiber optic equivalent of a Michelson interferometer, as shown in Figure 10. With this setup, only one bidirectional coupler is

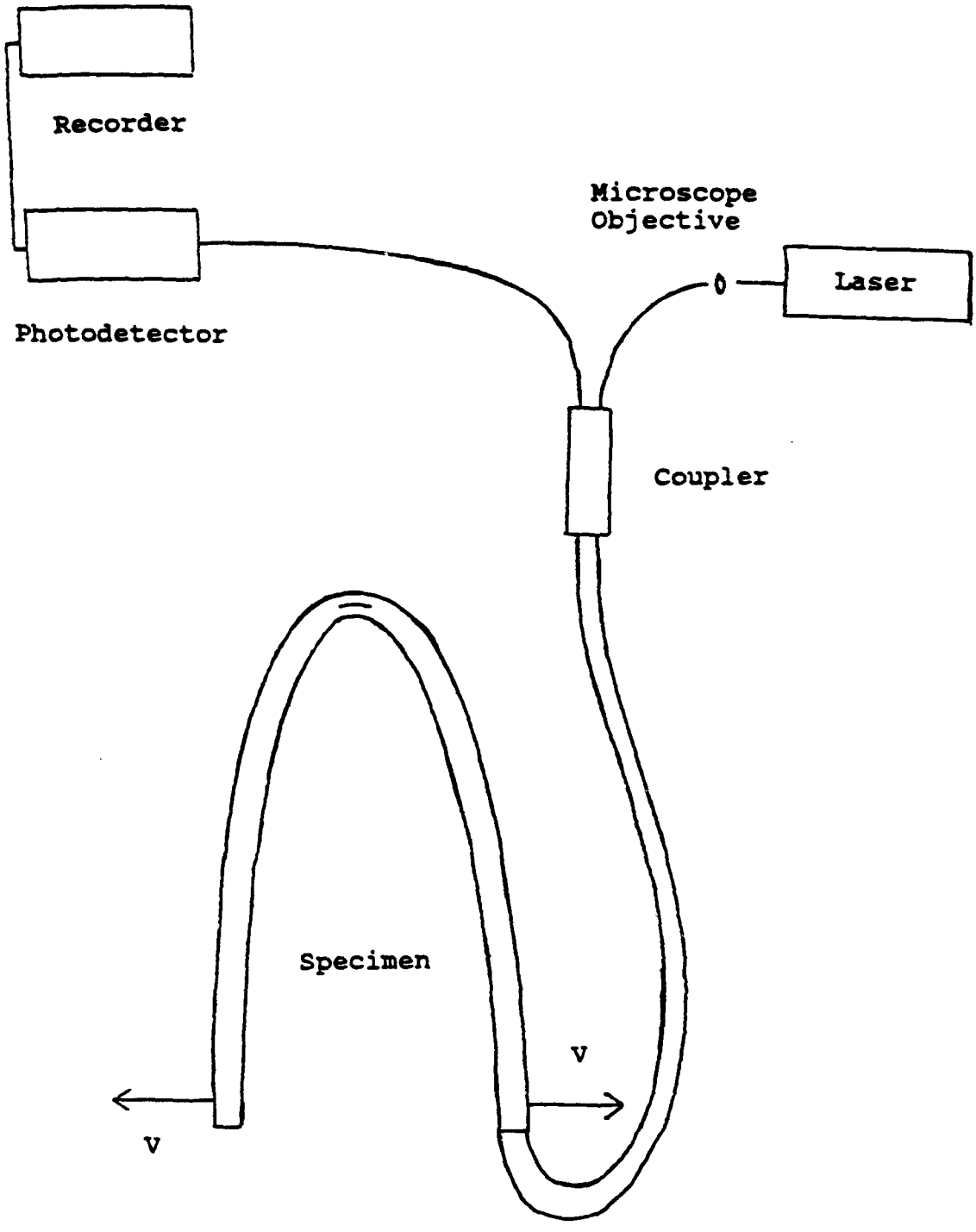

Figure 10. Optical fiber strain gage in configuration of Michelson interferometer

needed. The two optical arms of the interferometer are formed by two fibers from one end of a coupler on which mirrors had been deposited. Once a specimen has been tested, it can simply be broken off, and the two fibers re-silvered. This way, each sample only uses up a few inches of fiber attached to the bidirectional coupler. A bidirectional coupler was purchased with a pair of five meter fibers already attached to one end. As such, it can be reused dozens of times before needing to be replaced.

Moreover, it was found that the polarization problem inherent in the Mach-Zehnder configuration does not occur with the Michelson interferometer. This is because the light in each arm of the interferometer travels the same path twice, but in opposite directions. The changes in polarization that occur during the first passage are exactly cancelled by the changes that occur on the second. This effect is called "time reversal" in theoretical optics, and it makes possible a significant improvement over the optical fiber strain gage used in Midshipman Robinson's Trident Scholar research.

Construction of Michelson Interferometer

The mirrored surfaces required for a Michelson interferometer are formed by the deposition of aluminum on the cleaved ends of optical fibers using vacuum evaporation. This is done using a vacuum system consisting of a bell jar, a

mechanical pump, and a diffusion pump connected with valves between them as shown in Figure 11.

A diffusion pump works by vaporizing oil and causing the oil vapor to collide with air molecules and so drive them away from the bell jar towards the mechanical pump. If it has not been operating for some time, it must be warmed up for about thirty minutes. During this time, the bell jar can be removed and the fibers to be silvered are placed in the vacuum chamber. The vacuum chamber contains a tungsten filament with several small pieces of aluminum wire hanging from it, arranged so that the aluminum is in a straight line of sight with the fibers to be silvered.

To produce the vacuum in the bell jar, the backing valve is closed and the roughing valve is opened. This allows the mechanical pump to remove most of the air from the bell jar. After the pressure in the jar reaches a steady state (at about 50 millitorr), the roughing valve is closed and the backing valve is opened. This allows the mechanical pump to work on the outlet of the diffusion pump. Finally, the main valve is opened. This allows the mechanical pump and the diffusion pump to work in series to produce a very strong vacuum.

Once the vacuum is produced, a heavy current is run through the filament. This causes the aluminum on the filament to boil off and be deposited on everything within a straight line of sight of the filament, particularly the exposed ends of the optical fibers. After allowing the

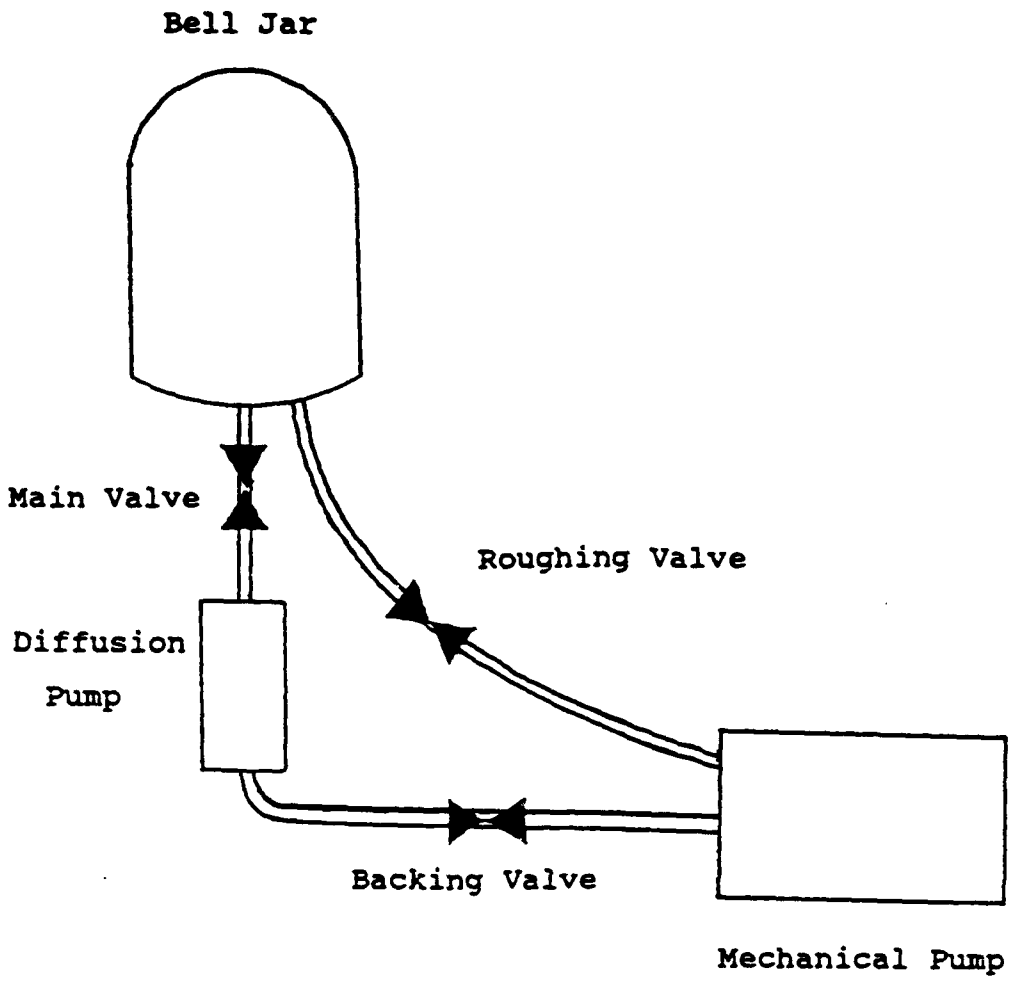

Figure 11. Vacuum system used to deposit aluminum mirrors onto optical fibers

filament to cool for a few minutes, the main valve is shut and the chamber is vented to bring it back to atmospheric pressure. The bell jar can then be lifted, and the coupler with the newly deposited mirrors can be removed.

In order to silver only the ends of the fibers, the sheet metal box shown in Figure 12 was built. This box can also be used to safely transport the coupler with its fragile mirrored surfaces from the vacuum system to another laboratory, where the rest of the experiment is conducted.

Because the reflecting surfaces are very fragile, the coupler with the new mirrored surfaces is first tested to see that it is an interferometer. Light is inserted into the input port of the coupler and detected by pointing the output port of the coupler at a nonspecular surface. Then one of the interferometer arms is moved slightly. If variations in light level are visible in diffuse reflection, an interferometer has been created.

The next step in the preparation of the specimen is the gluing of the interferometer arms onto the specimen. Once this is done, the mirrors are buried in epoxy resin and are quite stable. In more realistic experiments, the interferometer arms would be included in the specimen during the original lay-up. This is not practical in the present work for several reasons. For example, the mirrored surfaces and other interferometer components were very fragile, and could easily have been destroyed in the lay-up of the

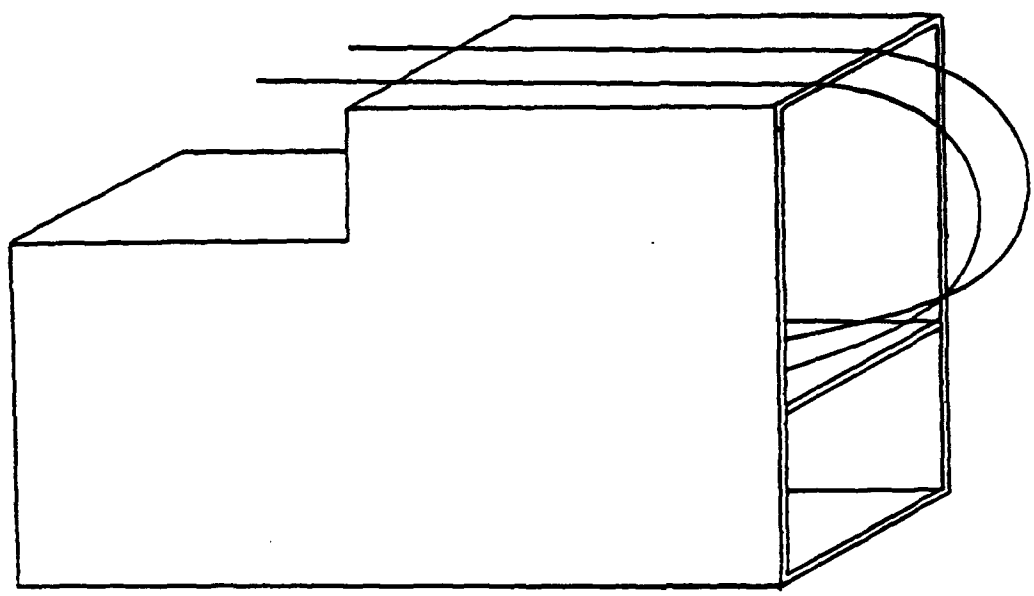

Figure 12. Box used to shield and transport optical fiber strain gage during vacuum deposition process

specimen. Because five or six specimens were cut from each initial lay-up of composite material, it would have required an equal number of couplers.

Optical Fringe Generation

The fringes at the output port of the optical coupler consist of light variations due to varying phases of the coherent light waves which are recombined in the coupler. The phases of the light beams are determined by the mechanical strains in the specimen to which the interferometer arms are attached. The relation between a phase change, $\Delta\phi$, and a strain, ϵ, in a length dx is given in Robinson's report and is repeated in Equation 3 below.[10]

$$\Delta\phi = \left(\frac{2\pi}{\lambda_0}\right) * (n-C) * (\epsilon dx) \qquad (3)$$

Here n = 1.5, the nominal index of refraction of the optical fiber core, and C = 0.165, a constant measured empirically by MIDN Robinson which is associated with the change in the index of refraction caused by the straining of a glass fiber.[11] When the strain is integrated over the total length of the specimen to which the fiber is attached, a total phase change is obtained. If ϕ_1 is the total phase change in one arm and

---

[10]Robinson, p. 19.

[11]Robinson, p. 23.

ϕ_2 is the total phase change in the other arm, the intensity of the light at the output port is that given in Equation 4, and this is proportional to the current in the solid state photodetector.[12]

$$i = E^2*(1+\cos(\phi_1-\phi_2)) = E^2*(1+\cos(2\pi*N)) \qquad (4)$$

In Appendices E, F, and G, the relation between the difference in the lengths of the two surfaces of the specimen and the displacement, u, of one end of the specimen relative to its center is derived. It is converted into N, the number of wavelengths, which is also the number of corresponding fringes. When the screw is turned through one-half rotation, each end of the specimen moves through (1/2) * (1/32) inches. The number of fringes estimated from these relations is 222. This compares with a measured number of between 150 and 200.

Electronic signal Processing

The photodetector is mounted in the circuit shown in Figure 13. This amplifies the signal as necessary and also has the provision for eliminating a DC level. At the output of this circuit, the signal was sent through an attenuator to a commercial cassette tape player/recorder where a permanent record was made. An amplifier with speakers and an oscilloscope are used to monitor the signals in real time.

---

[12]Robinson, p. 18.

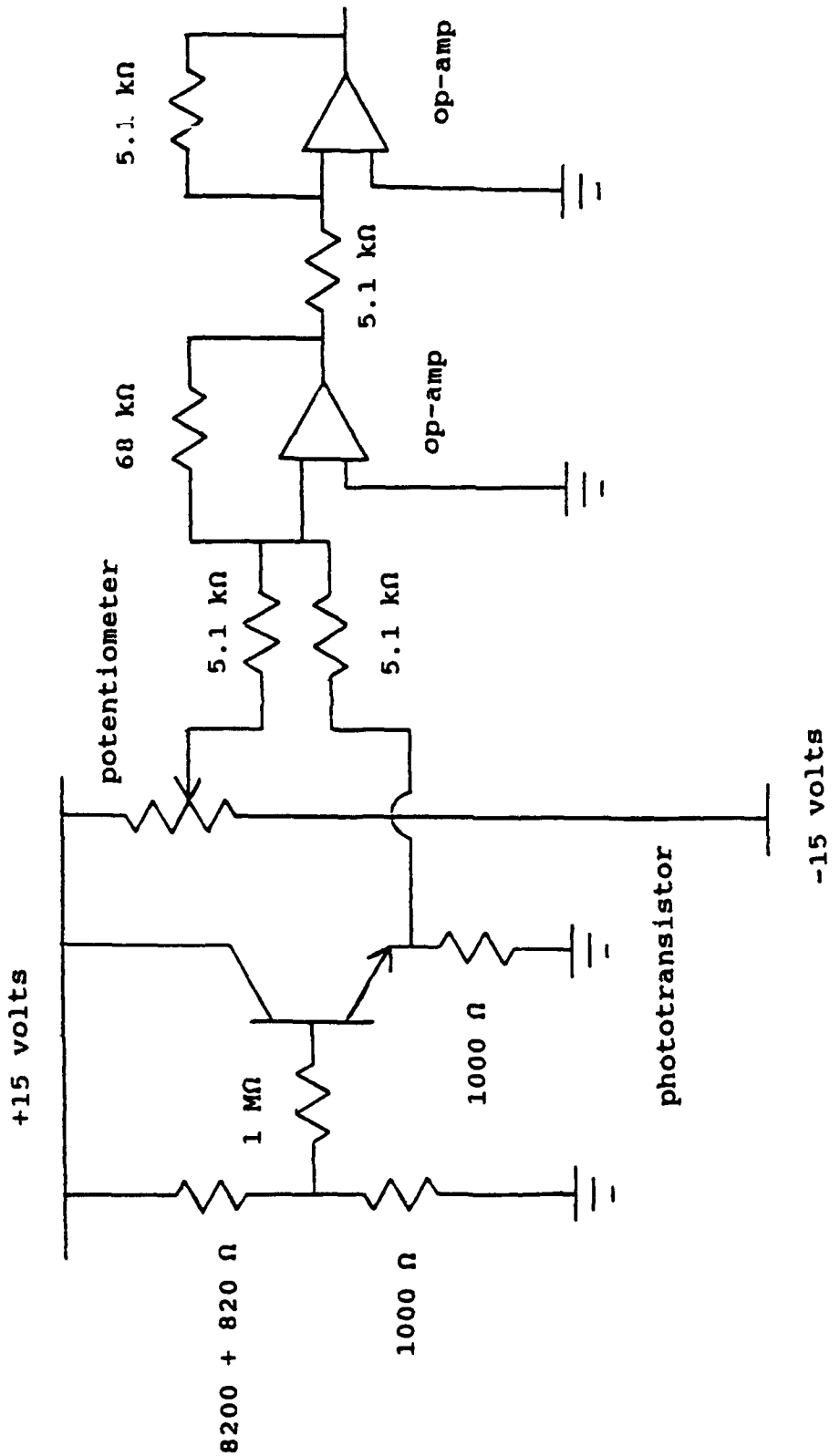

Figure 13. Electronic circuit for photodetector

The cassette on which the signals were recorded was played back on an identical audio system with a cassette tape player, amplifier, and speakers. The output to the speakers was connected to a digital recording oscilloscope. This information was then transferred to a digital computer using the programs listed in Appendix H. Using MATLAB software, these signal waveforms were plotted, printed, and analyzed.

Results

Typical plots of the recorded waveforms are shown in Figures 14 through 16. The varying amplitude of these waveforms contains no information on the experiment. As with any magnetic recording device, the amplitude of the signal depends on the frequency, and falls to zero as the signal frequency approaches zero. For this reason, a Fourier transform analysis and a power spectrum are not very useful. The useful information lies in the zero crossings.

Figures 14 shows the result of a typical half turn on the test apparatus. This turn was made at a fairly constant rate, and so the zero crossings of the waveform occur at fairly constant intervals. As mentioned earlier, the number of fringes counted in the waveforms were close to the predicted value.

Figure 15 is the plot of an actual delamination signal. When a specimen delaminates, it does so suddenly and

catastrophically. This plot shows the sudden occurrence of delamination. It also shows that the number of zero crossings of the waveform decrease and slow to a halt as the spreading of the delamination also comes to a stop. This waveform is very characteristic of a breakage, and is easily recognizable. It should be possible to create a matched filter device to detect this delamination signal.

After a major delamination has occurred, a waveform such as that shown in Figure 16 is present if the specimen is still deflected. This is interpreted as a continuing micro-delaminations. These micro-delaminations were never observed in an unbroken specimen, and were always observed in a broken and deflected specimen.

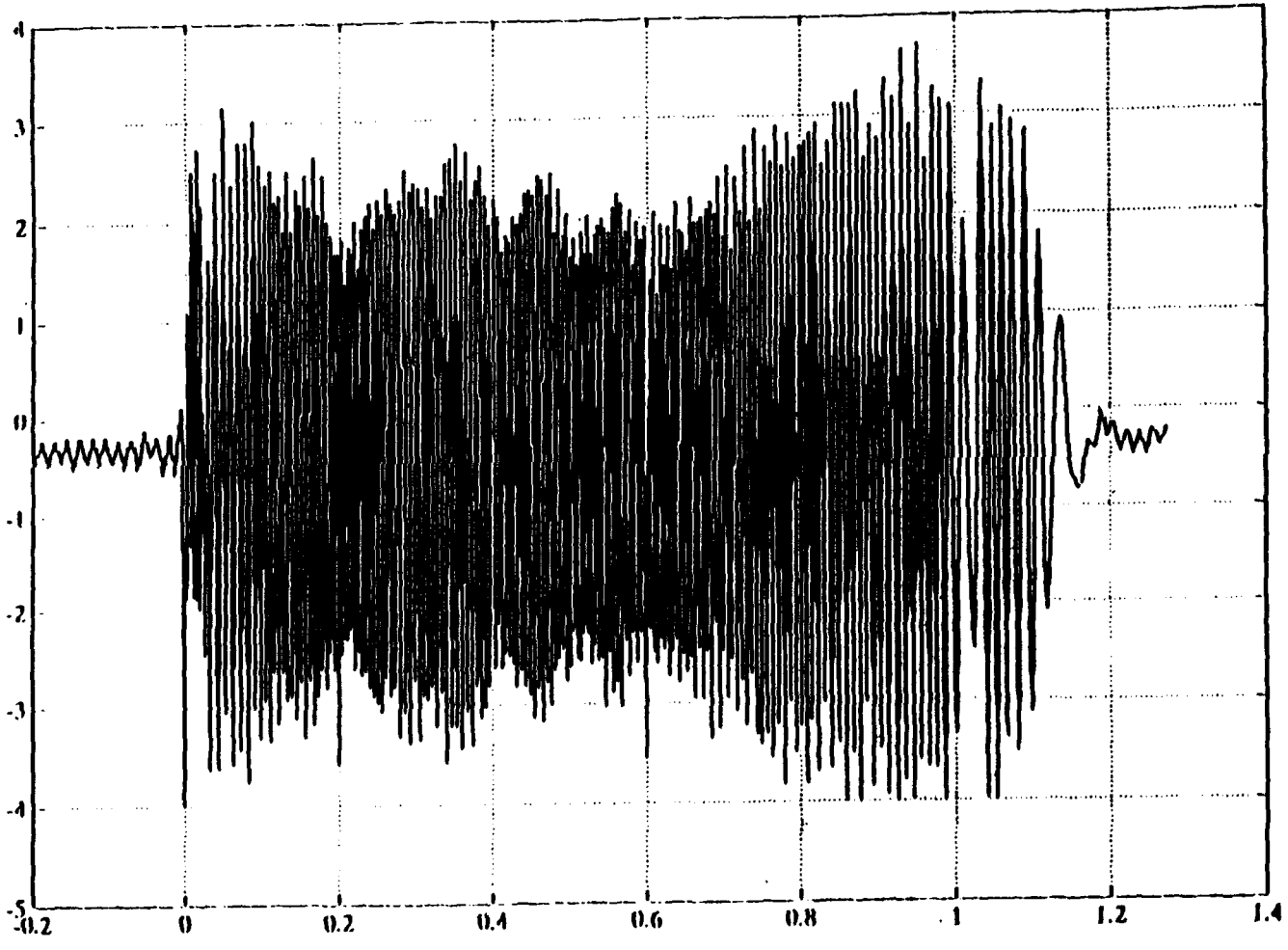

Figure 14. Waveform of a typical half-turn on the test apparatus

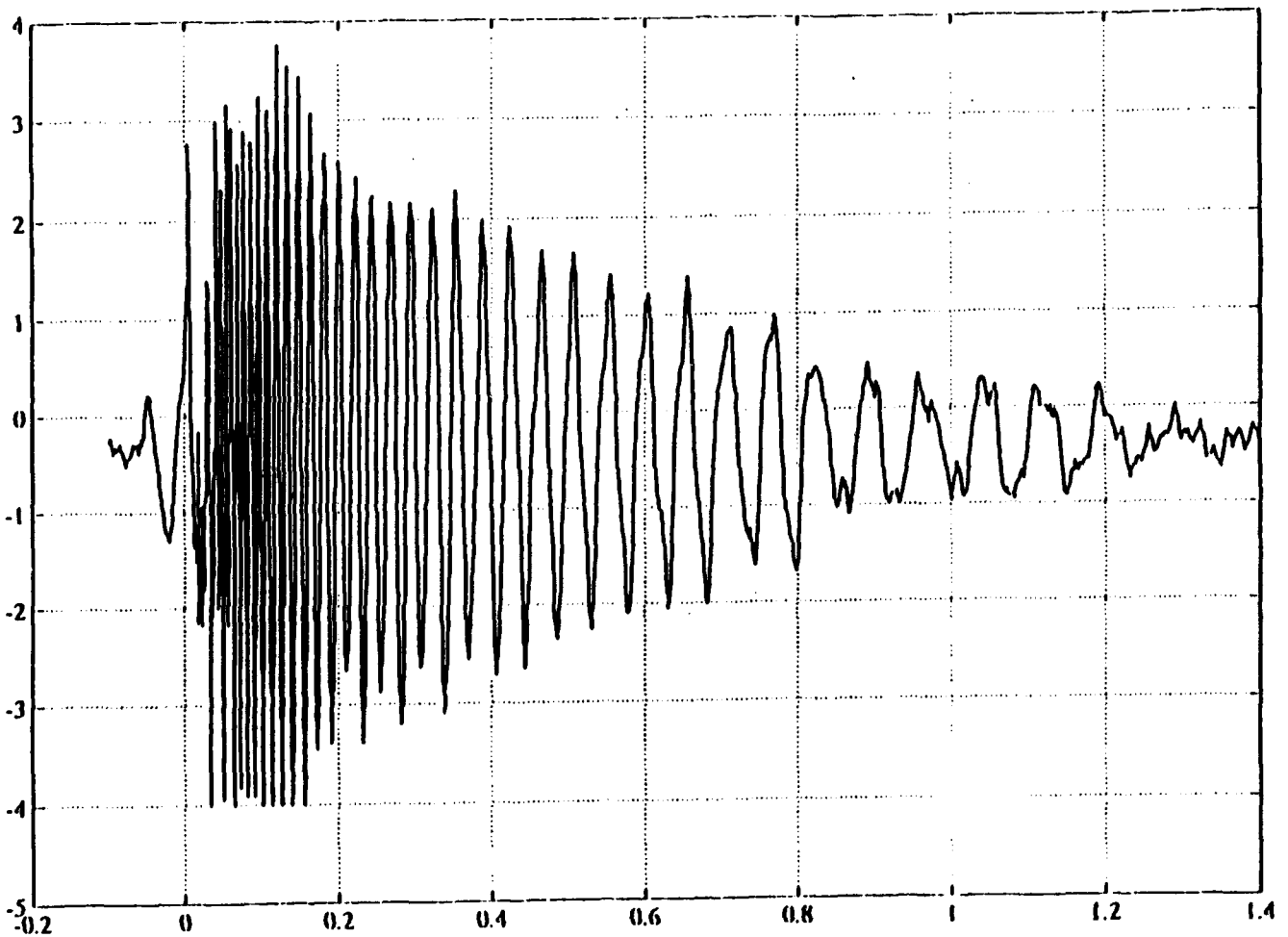

Figure 15. Waveform of a typical delamination

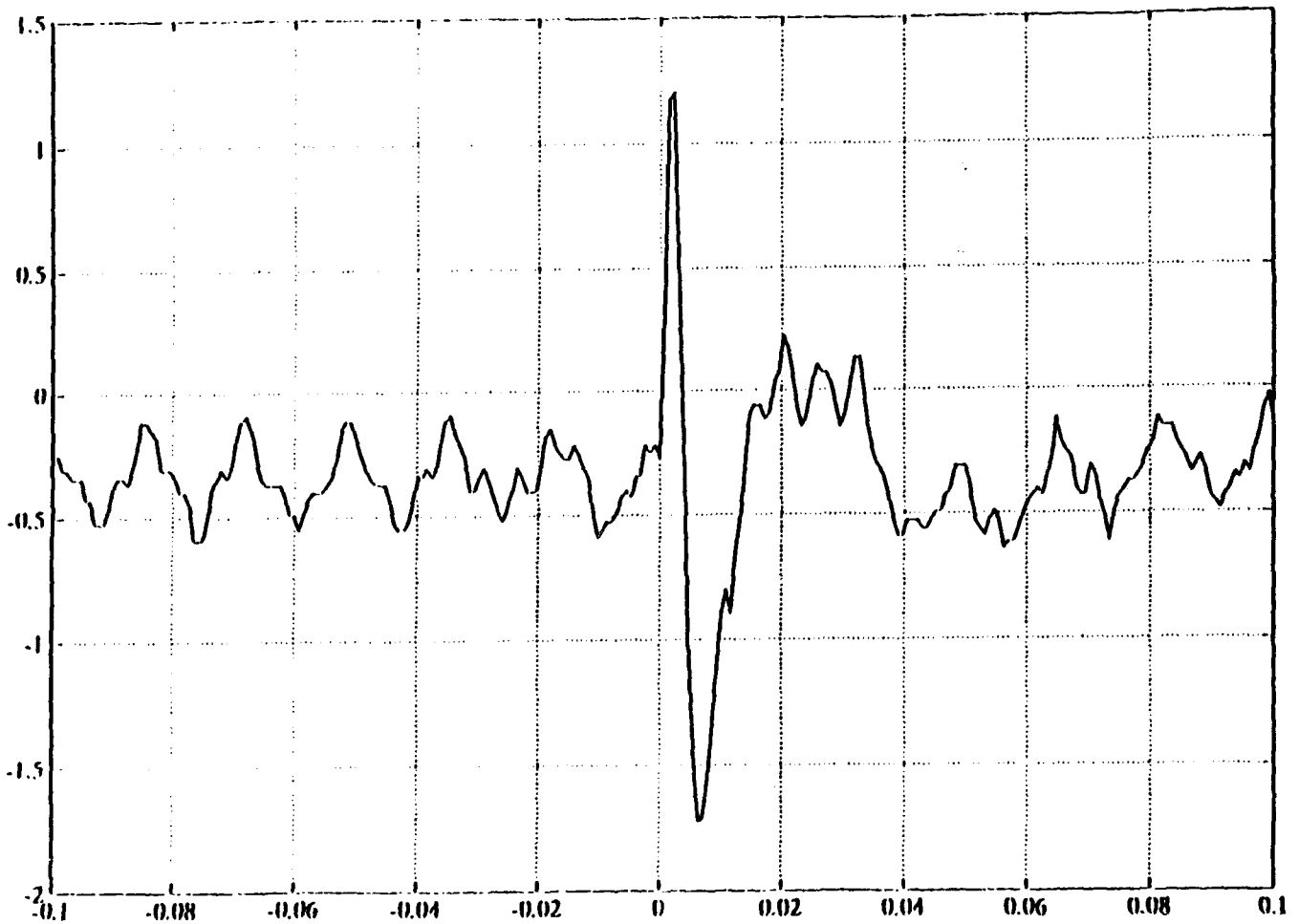

Figure 16. Waveform of a typical micro-delamination

Applications

One possible application of this work would be to use an optical fiber strain gage to test for prior delaminations. This could be done by applying some load to the structure, and checking for the presence of the micro-delaminations discussed above. If the waveform characteristic of micro-delaminations is observed, that is evidence that delamination has already occurred.

Another possible application would be a system to unload a structure in real time at the onset of delamination. For example, an optical fiber strain gage output could be attached through a matched filter to the auto-pilot control of an aircraft. As soon as signs of a delamination are detected, the auto-pilot could take action to maneuver the aircraft in such a way as to remove the stress causing the delamination.

Future Work

One possibility for future work involves a closer study of the delamination itself. The mathematics used to describe the specimen, either with or without stress, is well understood. However, once a delamination has occurred, these equations are no longer useful. A better model of the delaminated specimen could be obtained using finite element

analysis. This would also allow for a better interpretation of the signal obtained from an actual breakage.

Another area for future work is to improve the fiber optic strain gage configuration. The strain gage used in this project did not differentiate between positive and negative strains (tension and compression). However, by using feedback from the photo-detector to control the tension on the reference fiber of the interferometer, a phase locked loop could be produced, and the ambiguity eliminated. The setup for this device is shown in Figure 17.

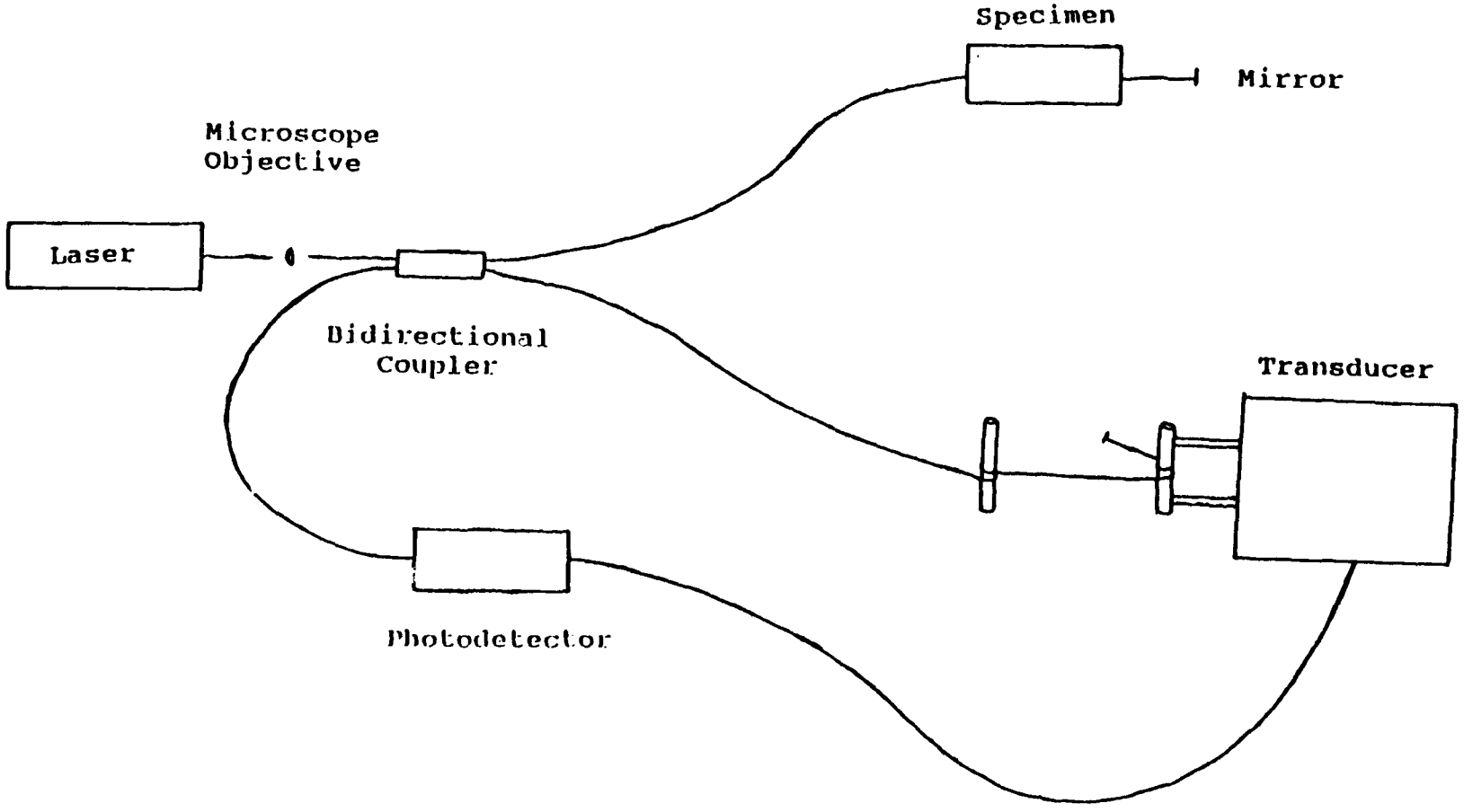

Figure 17. Improved fiber optic strain gage with feedback loop to eliminate positive/negative ambiguity

Bibliography

Agarwal, Bhagwan D. and Lawrence J. Broutman. Analysis and Performance of Fiber Composites. (New York: John Wiley & Sons, Inc., 1990).

Claus, Richard O. and Eric Udd. "Fiber Optic Smart Structures and Skins IV." SPIE. Vol 1588 (1991).

Dakin, John P. The Distributed Fibre Optic Sensing Handbook. IFS Publications: New York, 1990.

Dally, James W. and William F. Riley. Experimental Stress Analysis. McGraw-Hill Book Company: New York, 1978.

Griffith, A.A. "The Phenomena of Rupture and Flow in Solids." Philosophical Transactions Royal Society (London). Vol. 221 (Oct., 1920).

Hiel, Clement C., and Mark Sumich, and David P. Chappell. "A Curved Beam Test Specimen for Determining the Interlaminar Tensile Strength of a Laminated Composite." Journal of Composite Materials. Vol. 25 (July 1991).

Hong, S. and D. Liu. "On the Relationship Between Impact Energy and Delamination Area." Experimental Mechanics. Vol. 29 (June 1992).

Joh, Duksung. "A Semi-Micromechanic Interlaminar Strain Analysis on Curved-Beam Specimens." NASA Contractor Report. (1990).

Kedward, K.T. and R.S. Wilson and S.K. Mclean. "Flexure of Simply Curved Composite Shapes." Composites. Vol. 20, Num. 6. (Nov. 1989).

Kersey, A.D. and M.J. Marrone and A. Dandridge. "Input Polarization Effects on Interferometric Fiber-Optic Sensors." SPIE. Vol. 949 (1988).

Kim, C.G. and E.J. Jun. "Measurement of Impact Delamination by Deply Technique." Experimental Techniques. Vol. 16 (July/Aug. 1992).

Ko, William L. and Raymond H. Jackson. "Open-Mode Delamination Stress Concentrations in Horseshoe and Elliptic Composite Curved Bars Subjected to End Forces." NASA Technical Memorandum 4164. (1990).

Marine Composites. Eric Greene Associates, 1990.

Martin, Roderick H. "Analysis of Delamination Onset and Growth in Curved Laminates." (1991).

Peck, Scott O., and George S. Springer. "The Behavior of Delaminations in Composite Plates--Analytical and Experimental Results." Journal of Composite Materials. Vol 25 (July 1991).

Projects in Fiber Optics: Applications Handbook. Newport Corporation. 1986.

Robinson, Daniel B. "Optical Strain Monitoring in Composite Materials." Trident Scholar Project Report Num. 186. United States Naval Academy, 1991.

Sadat, A.B. and W.S. Chan and B.P. Wang. "Delamination of Graphite/Epoxy Laminate During Drilling Operation." Journal of Energy Resources Technology. Vol. 114 (June 1992).

Sumich, M. "Manufacture of Composite Test Specimens for Delamination Studies." Experimental Techniques. Vol. 13 (Oct. 1989).

Sumich, Mark and Keith T. Kedward. "Development of a Fatigue-Life Methodology for Composite Structures Subjected to Out-of-Plane Load Components." NASA Technical Memorandum 102885. (1991).

Suo, Z. and G. Bao and B. Fan. "Delamination R-Curve Phenomena Due to Damage." Journal of the Mechanics and Physics of Solids. Vol. 40 (Jan 1992).

Whitney, James M. "Stress Analysis of a Mode I Edge Delamination Specimen for Composite Materials." AIAA Journal. Vol. 24 (July 1986).

Appendix A

Longitudinal Shear Stress in the Bending of a Normally Straight Beam

The relation for longitudinal strain, ϵ_x, as a function of beam geometry is given in Equation 1 and illustrated in Figure A. R is the radius of curvature and z is the vertical distance from the center of the beam to the point of interest within the beam.

$$\epsilon_x = \frac{z}{R} \tag{1}$$

Using Hooke's law the corresponding stress can be calculated as shown in Equation 2.

$$\sigma_x = E_L * \epsilon_x = \frac{E_L}{R} * z \tag{2}$$

The basic equation for a bending beam is given in Equation 3.

$$\frac{E_L}{R} * I = M \tag{3}$$

Here M is the moment on the beam at the point of interest. The longitudinal stress, σ_x, in terms of the moment of inertia ,I, and z and M is given in Equation 4.

$$\sigma_x = \frac{M}{I} * z \tag{4}$$

Taking the volume of the beam from the point z to the surface which is over the length between s_o and s_1, the force, F_o, on the side at s_o is given in Equation 5.

$$F_o = \int_z^{t/2} \sigma_{x_0}\, dA = \int_z^{t/2} \left(\frac{M_o}{I}\right) * z * w * dz = \left(\frac{M_o}{I}\right) * w \int_z^{t/2} z\,dz \qquad (5)$$

Similarly, the force on the side at s_1 is given in Equation 6.

$$F_1 = \left(\frac{M_1}{I}\right) * w \int_z^{t/2} z\,dz \qquad (6)$$

The difference between these forces must be opposed by the interlaminar shear force acting at the level, z, within the beam.

$$F_1 - F_0 = \tau * (s_1 - s_o) * w = \frac{(M_1 - M_0)}{I} * w \int_z^{t/2} z\,dz \qquad (7)$$

The interlaminar shear is given in Equation 8.

$$\tau = \frac{M_1 - M_0}{s_1 - s_0} * \frac{1}{I} \int_z^{t/2} z\,dz = \frac{dM}{dx} * \frac{1}{1/12 * w * t^3} * 1/2\left((t/2^2) - z^2\right) \qquad (8)$$

When z is set equal to 0, the expression is a maximum, and so the maximum interlaminar shear occurs at the center, z=0. For the case of rectangular beams which are used in this experiment τ is given in Equation 9.

$$\tau = \frac{dM}{dx} * \left(\frac{3}{2}\right) * \left(\frac{1}{wt}\right) = \left(\frac{3}{2}\right) * \left(\frac{V}{A}\right) \qquad (9)$$

Here the derivative of the moment is expressed as the shear force, V, and A=w*t is the area of the beam cross section.

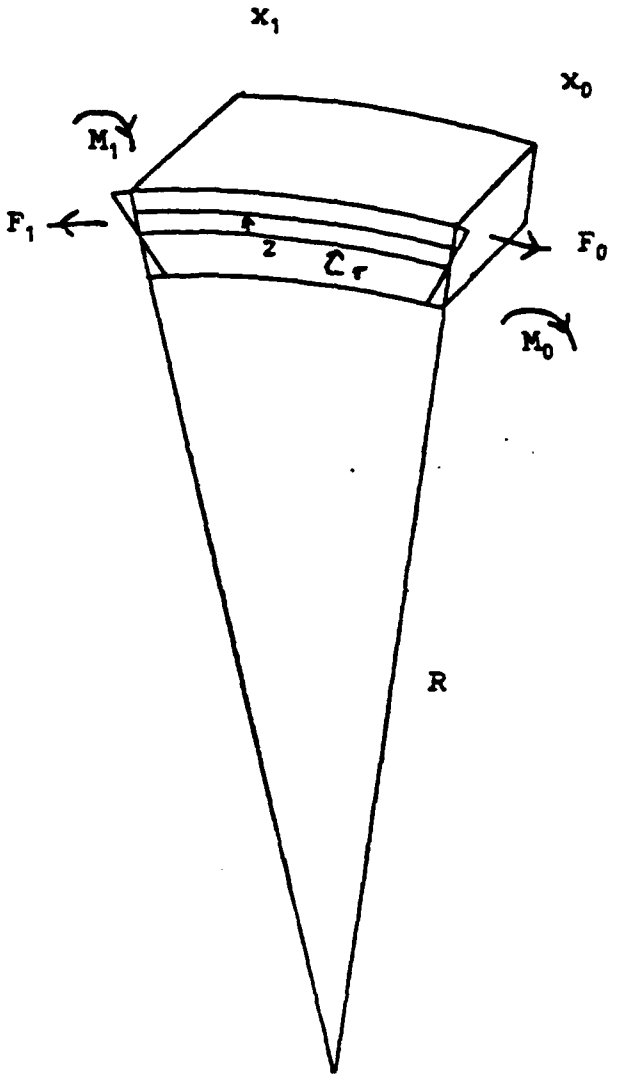

Figure A. Longitudinal Shear Stress in the Bending of a Normally Straight Beam

Appendix B

Transverse Stress in the Bending of a Normally Curved Beam

The section of a rectangular beam initially has a radius of curvature, R, a width, w, and a thickness, t. We consider a length of it, Δs, as shown in Figure B. The corresponding angle is θ. The beam is then bent. The angle changes and according to the figure the length of the beam, at the distance, z, from the center, changes the amount, δ. Equation 1 gives the relation between δ, z and $\Delta\theta$.

$$\delta = z*\Delta\theta \tag{1}$$

The curvature of the beam is the inverse of the radius of curvature.

$$\theta = \Delta s/R = \Delta s*K \qquad \Delta\theta = \Delta s*\Delta K \tag{2}$$

Uniting Equations 1 and 2, we have the relation in Equation 3.

$$\delta = z*\Delta s*\Delta K \qquad \frac{\delta}{\Delta s} = \epsilon_x = z*\Delta K \tag{3}$$

The longitudinal modulus of the material is termed, E_L, and Hook's law is given in Equation 4.

$$\sigma_x = E_L*\epsilon_x = E_L*z*\Delta K \tag{4}$$

The stress, σ_x, on an area, dz*w, causes the differential force, dP, along the beam which is given in Equation 5 .

$$dP = E_L * z * \Delta K * w * dz \tag{5}$$

If this force is integrated over half of the beam from z=0 to z=t/2, the result is as given in Equation 6.

$$P = E_L * \Delta K * w * \frac{t^2}{8} \tag{6}$$

The force, P, acts along the beam at the distance, Δs, from the center. Its vertical component is P*sin(θ) and since θ is assumed to be small, the transverse component is as given in Equation 7 .

$$P_T = E_L * \Delta K * w * \frac{t^2}{8} * \theta = E_L * \Delta K * w * \frac{t^2}{8} * \frac{\Delta s}{R} \tag{7}$$

Since the area normal to this force is the product, w*Δs, the stress normal to the beam is shown in Equation 8. From the development it can be seen to have a maximum at z=0, the center of the beam.

$$\frac{P_V}{\Delta s * w} = \sigma_T = E_L * \frac{t^2}{8} * \frac{\Delta K}{R} \tag{8}$$

This relation gives the transverse stress within a beam as a function of its modulus, its initial radius of curvature, R , its thickness, t, and the change of curvature, ΔK, which is imposed upon it to create the stress.

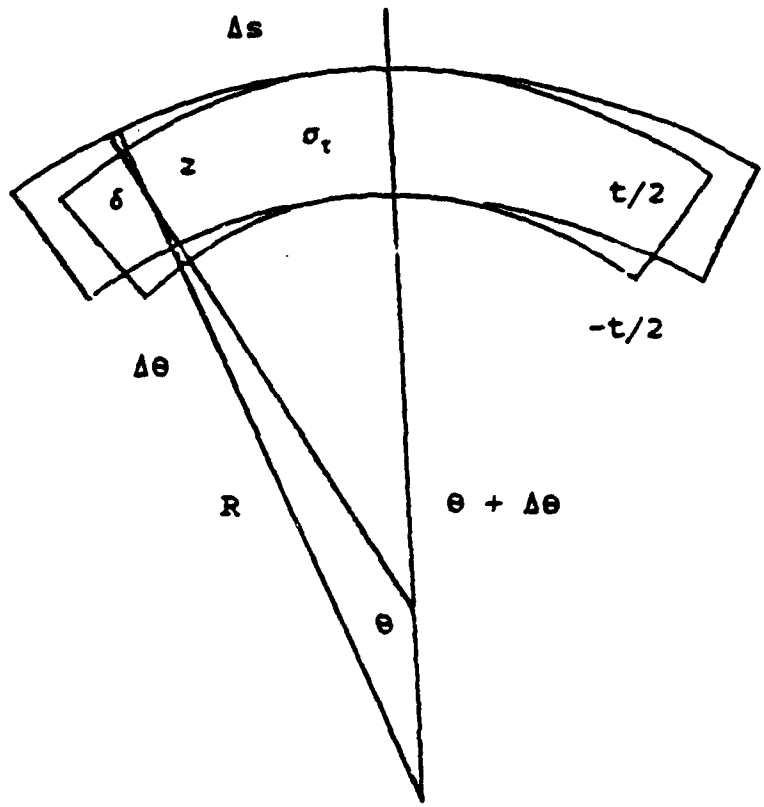

Figure B. Transverse Stress in the Bending of a Normally Curved Beam

Appendix C

Radius of Curvature on the Elliptical Test Specimen

The specimen chosen for test is illustrated in Figure C. It is one half of an ellipse with the dimensions shown in the figure. The equation for the figure is given in Equation 1.

$$\frac{x^2}{a^2}+\frac{y^2}{b^2}=1 \qquad y=b*\left(1-\frac{x^2}{a^2}\right)^{1/2} \tag{1}$$

The first derivative is given in Equation 2.

$$\frac{dy}{dx}=-\frac{b}{a^2}*\left(\frac{x}{\left(1-\frac{x^2}{a^2}\right)^{1/2}}\right)=-\frac{b^2}{a^2}*\frac{x}{y} \tag{2}$$

The second derivative is given in Equation 3.

$$\frac{d^2y}{dx^2}=-\frac{b}{a^2}*\left(\frac{1}{\left(1-\frac{x^2}{a^2}\right)^{3/2}}\right)=-\frac{b^4}{a^2*y^3} \tag{3}$$

The expression for the curvature, K, of a function is given in Equation 4.

$$K=\frac{\frac{d^2y}{dx^2}}{\left(1+\left(\frac{dy}{dx}\right)^2\right)^{3/2}} \tag{4}$$

When the expressions for the first and second derivatives are substituted into Equation 4 the expression for K is as shown in Equation 5.

$$K=\frac{-\frac{b}{a^2}}{\left(1+x^2*\left(\frac{b^2-a^2}{a^4}\right)\right)^{3/2}} \qquad (5)$$

When the expression in Equation 5 is evaluated at x=0, we get $K=-b/a^2$. When it is evaluated at x=a, we get $K= -a/b^2$. In the experiment, a=0.75 inches and b=3.00 inches. The two values of curvature are 5.33 and .083 in units of $inches^{-1}$.

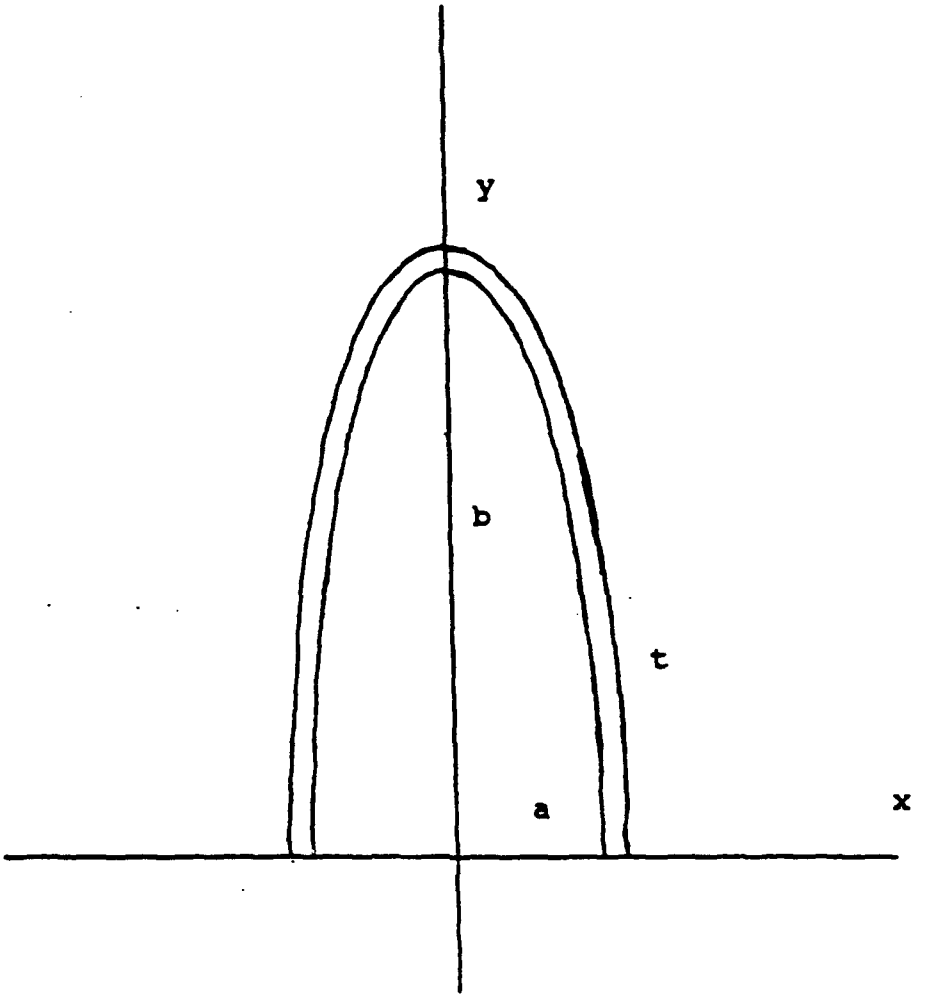

Figure C. Elliptical Test Specimen

Appendix D

Generation of Interlaminar Stress

The shear stress in the center of a straight beam in bending is a maximum in the center of the beam at the fixed end as illustrated in Figure D1. In Appendix A it was shown to be given by the expression in Equation 1.

$$\tau = (\frac{3}{2}) * (\frac{V}{A}) \qquad (1)$$

Here τ is the shear force per unit area, A is the area of the cross section of the beam and V is the applied force.

The transverse stress in the center of the apex of the elliptical specimen which is illustrated in Figure D2 was shown in Appendix B to be given by the expression in Equation 2.

$$\sigma_T = E_L * \frac{t^2}{8} * \frac{\Delta K}{R} \qquad (2)$$

The general relation between beam geometry and applied moment is given in Equation 3.

$$\frac{E_L * I}{R} = M \qquad E_L * I * K = M \qquad E_L * I * \Delta K = \Delta M \qquad \Delta K = \frac{\Delta M}{E_L * I} \qquad (3)$$

If the expressions for the moment of inertia, I, of a rectangular beam and the applied curvature, ΔK, are substituted into Equation 2, the resulting expression in Equation 4 can be readily compared with Equation 1.

$$\sigma_T = E_L * \frac{t^2}{8} * \frac{\Delta M}{E_L * I} * \frac{1}{R} = \left(\frac{3}{2}\right) * \left(\frac{V}{A}\right) * \left(\frac{b^2}{a^2}\right) \qquad (4)$$

In the experiment, b=3.00 inches and a=0.75 inches. Therefore, there was a transverse stress, σ_T, in the elliptical beam which was sixteen times greater than τ, the maximum shear stress which was available in the straight beam.

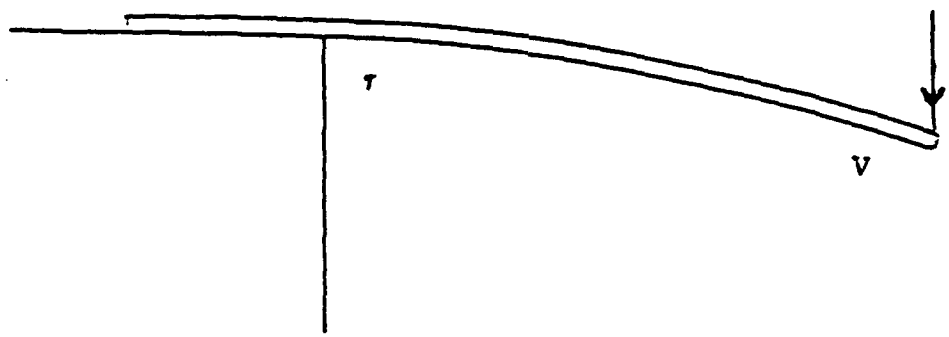

Figure D1. Interlaminar Shear Stress

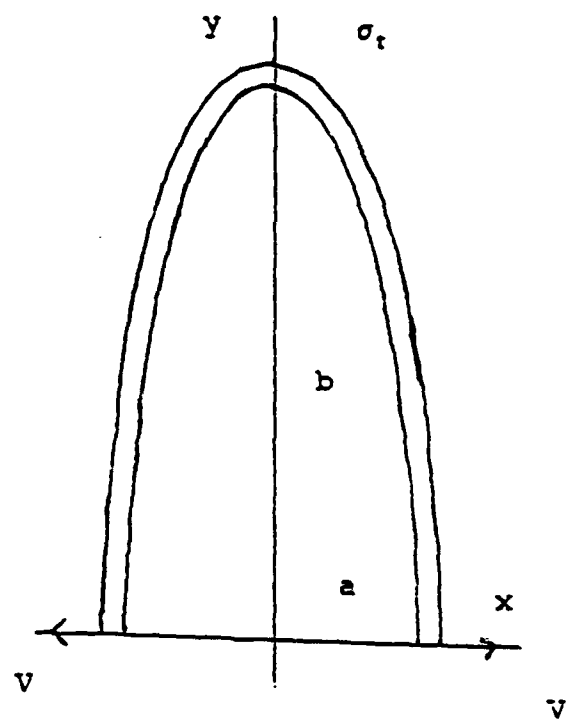

Figure D2. Interlaminar Transverse Stress

Appendix E

Change in Length of Specimen Surface with Forces Applied to Ends

The experimental arrangement is shown in Figure E. Applying Equation 3 in Appendix B, with z set equal to t/2, we get, δ, the change in length of Δs on its inner surface.

$$\delta = \frac{t}{2} * \Delta s * \Delta k \qquad (1)$$

Using Equation 3 in Appendix D, we get the relation in Equation 2.

$$\delta = \frac{t}{2} * \Delta s * \frac{\Delta M}{E_L * I} = \frac{t}{2} * \Delta s * \frac{\Delta F * y}{E_L * I} \qquad (2)$$

The increase in moment is the product of the increase in force, ΔF with the vertical distance, y. The distance, y, is given in terms of the distance, x, by the relation in Equation 1 of Appendix C. The distance, Δs, is expressed in terms of Δx by the expression in Equation 3.

$$\Delta s = \Delta x * \sqrt{1 + \left(\frac{dy}{dx}\right)^2} \qquad (3)$$

These relations result in the expression in Equation 4.

$$\delta = \frac{t}{2} * dx * \sqrt{1 + \left(\frac{dy}{dx}\right)^2} * \frac{1}{E_L * I} * \Delta F * b * \sqrt{1 + \frac{x^2}{a^2}} \qquad (4)$$

Equation 2 of Appendix C gives the relation for the derivative, dy/dx, on an ellipse. When it is substituted into Equation 4, and the result is simplified, the result is given in Equation 5.

$$\delta = \frac{t*b}{2*E_L*I}*\Delta F*dx*\sqrt{1+x^2*(\frac{b^2-a^2}{a^4})} \qquad (5)$$

When this expression is integrated from x=0 to x=.75 with the values of b=3.00 inches and a=.75 inches included and then doubled so as to include the domain of x from 0 to -.75 , the result is that given in Equation 6.

$$L = t*\frac{\Delta F}{E_L*I}*5.10 \qquad (6)$$

Here L is the total change in the length of the surface of the specimen, from one end to the other over the arch, E_L is its modulus and I is the moment of inertia of the specimen cross section.

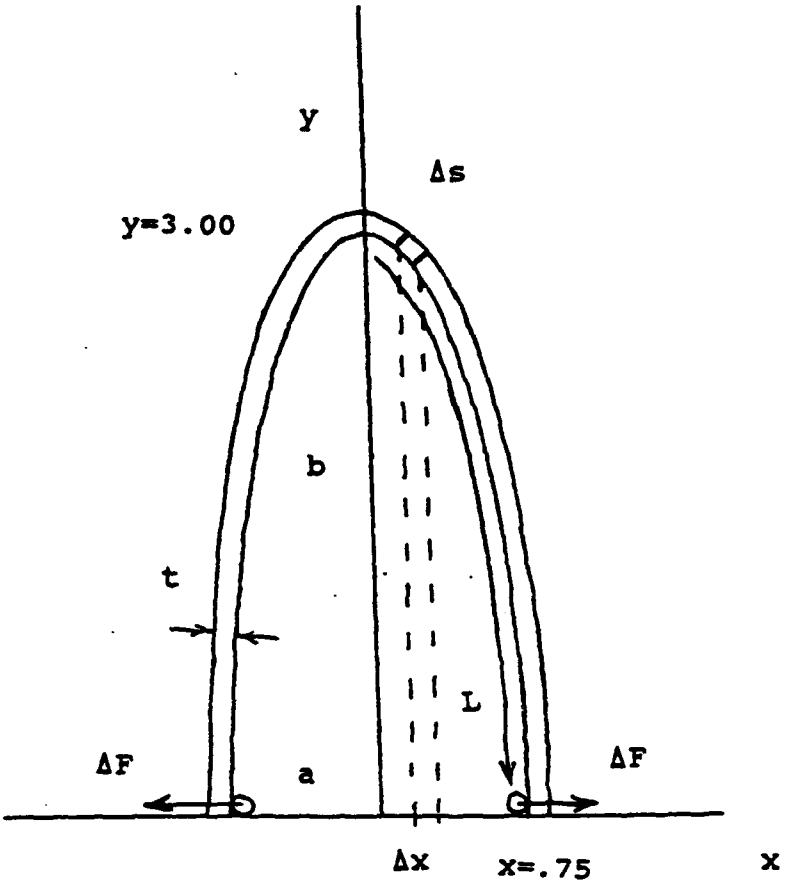

Figure E. Change in Length of Specimen Surface

Appendix F

Stiffness of Elliptical Specimen

Equation 2 of Appendix B relates the change in θ to the distance along the specimen and the change in curvature.

$$\Delta\theta = \Delta s * \Delta K \tag{1}$$

From Figure F, the distance, r, is seen to be given by the expression in Equation 2.

$$r^2 = (a-x)^2+y^2 \qquad r=\sqrt{(a-x)^2+y^2} \tag{2}$$

The angle, ϕ, in the diagram is given in Equation 3.

$$\varphi = \arctan\left(\frac{a-x}{y}\right) \tag{3}$$

With substitutions used previously, Equation 1 becomes Equation 4.

$$\Delta\theta = dx * \sqrt{1+\left(\frac{dy}{dx}\right)^2} * \frac{\Delta F * y}{E_L * I} \tag{4}$$

The distance, Δu, shown in Figure F is given in Equation 5.

$$\Delta u = (\Delta T) * \cos(\varphi) = (r * \Delta\theta) * \cos(\varphi) \tag{5}$$

When Equation 3 and Equation 4 are substituted into Equation 5, we obtain Equation 6.

$$\Delta u = \sqrt{(a-x)^2+y^2} * dx * \sqrt{1+\left(\frac{dy}{dx}\right)^2} * \frac{\Delta F * y}{E_L * I} * \cos\left(\arctan\left(\frac{a-x}{y}\right)\right) \quad (6)$$

The final substitution is to express dy/dx as in Equation 2 in Appendix C. The result is Equation 7.

$$\Delta u = \frac{\Delta F}{E_L * I} * dx * \sqrt{(a-x)^2+y^2} * \sqrt{1+\frac{b^4}{a^4} * \frac{x^2}{y^2}} * y * \cos\left(\arctan\left(\frac{a-x}{y}\right)\right) \quad (7)$$

This expression can be numerically integrated over x from x=0 to x=.75. The result is given in Equation 8.

$$u = \frac{\Delta F}{E_L * I} * 10.7 \quad (8)$$

Here u is the horizontal displacement of one end of the specimen, ΔF is the applied force, E_L is the modulus of the unidirectional composite and I is the moment of inertia of the specimen cross section.

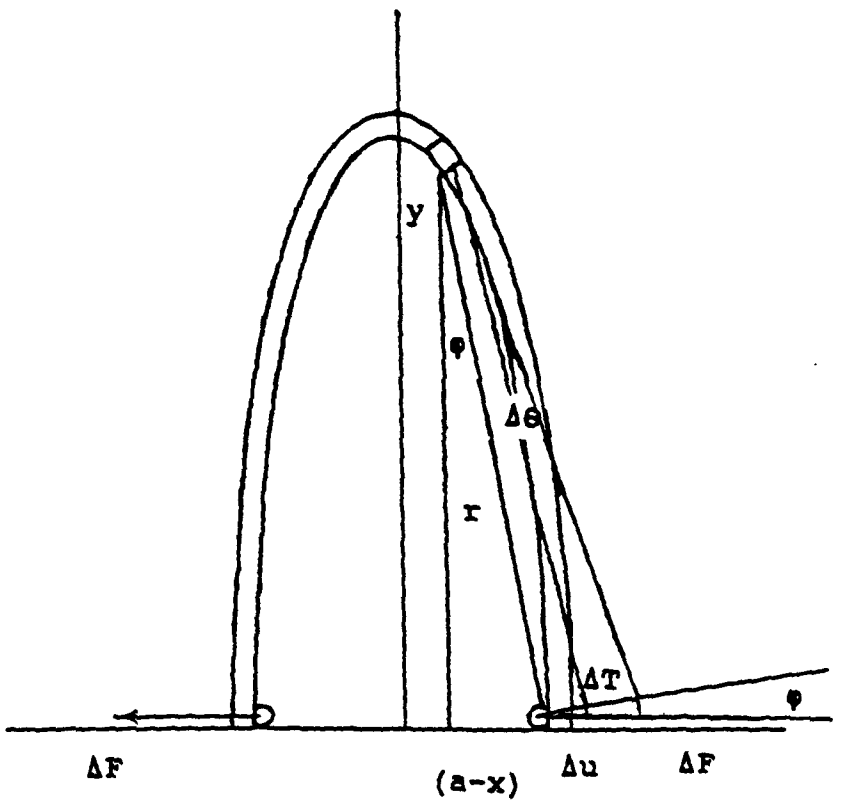

Figure F. Stiffness of Elliptical Specimen

Appendix G

Generation of Current Peaks

The results of Appendices E and F can be united to estimate the number of current peaks generated by the optical strain gage in the deflection of the unbroken specimen. Equation 6 of Appendix E gives the change in the length of one of the surfaces of the specimen in terms of the applied force. Since both top and bottom surfaces are traversed twice in the Michelson interferometer and since the sign of the change in length of one surface is opposite to that of the other surface, the length difference is four times that given in the equation. This is given in Equation 1.

$$\Delta L = 4*t*\frac{\Delta F}{E_L*I}*5.1 \qquad (1)$$

Equation 8 in Appendix F gives the displacement, u, of one of the specimen ends as a function of the applied force, ΔF. This is solved for ΔF and repeated in Equation 2.

$$\Delta F = u*E_L*I*(\frac{1}{10.7}) \qquad (2)$$

When Equation 2 is substituted into Equation 1 we get an expression for the difference in the length changes of each side of the specimen corresponding to the displacement, u, of one end on the specimen relative to its center.

$$\Delta L = 4*t*u*(\frac{5.1}{10.7}) \quad (3)$$

The thickness of the specimens is typically .140 inches. One half turn of the screw displaced the one end 1/32 inch and since this is split between both ends, the value for u in this case is 1/64 inches. Equation 4, taken from Midn Robinson's Trident report, gives the effective wavelength of a helium-neon laser in inches.

$$\lambda_e = 25*\frac{10^{-6}}{n-.165} \quad (4)$$

Here n = 1.5 which is the nominal index of refraction of the glass core and the constant, .165, is an empirically measured constant associated with the use of fiber optics as a strain gage. Dividing ΔL by λ_e, with the above values substituted, the number of current peaks is 222.

Appendix H

Computer Programs

The following is a copy of a PASCAL program used to transfer a waveform from the HP-54501a Digitizing Oscilloscope to a file on a digital computer.

```
program wave(input, output);

{read of 256 point waveform on channel 1 of scope}
{ write of waveform and scale factors to file scopedat.m}

type
          lstr4     =    lstring(4);
          lstr7     =    lstring(7);
          lstr14    =    lstring(14);
          ar256     =    array[1..256] of lstr7;

var
          i         :    integer;
          dfile     :    text;
          yr        :    ar256;
          result    :    lstr14;

{-------------------------------------------------}

procedure initialize;external;

procedure scope_setup;external;

procedure each_scale_factor(arg:lstr4;n:integer;
          var result:lstr14);external;

procedure read_waveform(var yr:ar256);external;

procedure wrapup;external;

{-------------------------------------------------}
```

```
procedure scale_factors;

begin

     each_scale_factor('xinc',4,result);
     writeln(dfile,'xinc=',result,';');
     each_scale_factor('xor',3,result);
     writeln(dfile,'xor=',result,';');
     each_scale_factor('xref',4,result);
     writeln(dfile,'xref=',result,';');
     each_scale_factor('yinc',4,result);
     writeln(dfile,'yinc=',result,';');
     each_scale_factor('yor',3,result);
     writeln(dfile,'yor=',result,';');
     each_scale_factor('yref',4,result);
     writeln(dfile,'yref=',result,';');
end;

{-------------------------------------------------------}

begin          {  main program  }

     initialize;
     assign(dfile,'scopedat.m');
     rewrite(dfile);
     scope_setup;
     scale_factors;
     read_waveform(yr);
     writeln(dfile,'yp=[');
     for i:=1 to 256 do
     begin
               writeln(dfile,yr[i]);
     end;
     writeln(dfile,'];');
     close(dfile);
     wrapup;
end.
```

The following is a copy of a MATLAB file that utilizes the above PASCAL file to take the data from the computer file, and put it into two vectors on MATLAB, x and y.

```
%file wave.m          read of HP-54501a scope
%
!wave                 %PASCAL version
scopedat;             %read of data file
n=length(yp);         %size of vector of data
dp=[1:n]';            %data point number
x = (dp-ones(dp)*xref)*xinc+xor*ones(dp);     %x axis
y = (yp-ones(yp)*yref)*yinc+yor*ones(yp);     %y axis
tv = input ('Plot title? ','s');
plot (x,y)
title(tv);
grid;
```

Acknowledgements

For their generous help in completing this project, I would like to thank the following people:

Prof. Olaf Rask, Systems Engineering

Mr. Tom Price, Technical Support

Prof. John Fontanella, Physics

Prof. Dennis Hasson, Mechanical Engineering

Prof. Robert DeMoyer, Systems Engineering

Prof. Terry Dwan, Systems Engineering

Mr. Sam Hawkins, Technical Support

Mr. Clyde Atwell, Technical Support